

**Title**

**Fabrication and characterisation of a  
novel MOSFET gas sensor**

Final thesis at Linköpings Institute of Technology  
performed at Fraunhofer Institute for Physical Measurement Techniques  
by

**Johan Dalin**

LITH-ISY-EX-3184



**Title**

**Fabrication and characterisation of a  
novel MOSFET gas sensor**

Final thesis at Linköpings Institute of Technology  
performed at Fraunhofer Institute for Physical Measurement Techniques  
by

**Johan Dalin**

LiTH-ISY-EX-3184

Tutor: **Jürgen Wöllenstein**

Fraunhofer Institute for Physical Measurement Techniques

**Lars Nielsen**

Linköpings Institute of Technology

Examiner: **Lars Nielsen**

Linköpings Institute of Technology

Freiburg 2002-06-05



	<b>Avdelning, Institution</b> Division, Department  Institutionen för Systemteknik 581 83 LINKÖPING	<b>Datum</b> Date 2002-06-05
<b>Språk</b> Language Svenska/Swedish X Engelska/English	<b>Rapporttyp</b> Report category Licentiatavhandling X Examensarbete C-uppsats D-uppsats Övrig rapport _____	<b>ISBN</b>  <b>ISRN</b>  <b>Serietitel och serienummer</b> <b>ISSN</b> Title of series, numbering    _____  LITH-ISY-EX-3184
<b>URL för elektronisk version</b> <a href="http://www.fs.isy.liu.se/">http://www.fs.isy.liu.se/</a>		
<b>Titel</b> Title  <b>Författare</b> Author	Tillverkning och karaktärisering av en ny MOSFET-gassensor  Fabrication and characterisation of a novel MOSFET gas sensor  Johan Dalin	
<b>Sammanfattning</b> Abstract  <p>A novel MOSFET gas sensor for the investigation has been developed. Its configuration resembles a "normally on" n-type thin-film transistor (TFT) with a gas sensitive metal oxide as a channel. The device used in the experiments only differs from common TFTs in the gate configuration. In order to allow gas reactions with the SnO<sub>2</sub>-surface, the gate is buried under the semiconducting layer. Without any gate voltage, the device works as a conventional metal oxide gas sensor. Applied gate voltages affect the channel carrier concentration and surface potential of the metal oxide, thus causing a change in sensitivity. The results of the gas measurements are in accordance with the electric adsorption effect, which was postulated by Fedor Wolkenstein 1957, and arises the possibility to operate a semiconductor gas sensor at relatively low temperatures and, thereby, be able to integrate CMOS electronics for processing of measurements at the same chip.</p>		
<b>Nyckelord</b> Keywords MOSFET gas sensor, Wolkenstein Model, CMOS integration		



## **ABSTRACT**

A novel MOSFET gas sensor for the investigation has been developed. Its configuration resembles a "normally on" n-type thin-film transistor (TFT) with a gas sensitive metal oxide as a channel. The device used in the experiments only differs from common TFTs in the gate configuration. In order to allow gas reactions with the SnO<sub>2</sub>-surface, the gate is buried under the semiconducting layer. Without any gate voltage, the device works as a conventional metal oxide gas sensor. Applied gate voltages affect the channel carrier concentration and surface potential of the metal oxide, thus causing a change in sensitivity. The results of the gas measurements are in accordance with the electric adsorption effect, which was postulated by Fedor Wolkenstein 1957, and arises the possibility to operate a semiconductor gas sensor at relatively low temperatures and, thereby, be able to integrate CMOS electronics for processing of measurements at the same chip.

## ACKNOWLEDGEMENTS

Herbert Verhoeven, Mirko Lehmann and Heinz-Peter Frerichs at Micronas and Jürgen Wöllenstein at Fraunhofer IPM have given me an interesting final thesis. I have always been fascinated to microelectronics.

For all laboratory work in the cleaning room I am grateful for all support I have received. To Marie-Louise Bauersfeld for learning me the routines, to Emmanuel Moreton for enjoyable moments at the sputtering machine, to Gerd Kühner for solutions when something made a bother, to Angela Pohlmann, Christa Künzel and Ursula Bartsch for their wise advises and work, to Stefan Palzer for giving valuable support to bond the chips and, finally, to Gerd Plescher for regular help at the scanning electron microscope.

Together with Sven Rademacher, Patrick Auer, Marie-Louise Bauersfeld and Jürgen Hildebrand the work atmosphere was very relaxed and professional, which I appreciate. My tutor at Fraunhofer Institute, Jürgen Wöllenstein, is worth all credits for patient and good co-operation.

My examiner, Lars Nielsen, for showing interest for my work.

Finally, I want to thank;  
Martin Jäggle, who gave me an interesting first day at Fraunhofer Institute,  
Harald Böttner for valuable advises,  
Armin Kiefer for support with the electronic construction.

# TABLE OF CONTENTS

<b>1. INTRODUCTION .....</b>	<b>1</b>
<b>2. THEORY OF A METAL-OXIDE-SEMICONDUCTOR FIELD EFFECT TRANSISTOR.....</b>	<b>5</b>
<b>2.1 Introduction.....</b>	<b>5</b>
<b>2.2 Physical description of a MOSFET.....</b>	<b>6</b>
2.2.1 Doping of semiconductors .....	6
2.2.2 Equilibrium state of a semiconductor.....	7
2.2.3 N-channel of an n-type MOSFET .....	9
2.2.4 Potential variation from gate to substrate of an n-type MOSFET influenced by an electric field.....	11
2.2.5 Potential variation from source to drain of an n-type MOSFET influenced by an electric field.....	12
<b>3. GAS SENSING PROPERTIES OF AN INSULATED-GATE THIN-FILM TIN DIOXIDE TRANSISTOR.....</b>	<b>15</b>
<b>3.1 Gas sensing properties of tin dioxide.....</b>	<b>15</b>
3.1.1. Definition of thin-film transistor.....	15
3.1.2 Characteristics of Insulated-gate thin-film transistors .....	15
3.1.3 Semiconductor properties of tin dioxide .....	16
3.1.4 Nitrogen oxides and carbon monoxide .....	17
3.1.5 Principles of nitrogen oxides and carbon monoxide measurement .....	18
<b>3.2 Control selectivity and sensitivity .....</b>	<b>22</b>
3.2.1 Methods .....	22
3.2.2 Control by external electric field.....	23
3.2.3 Wolkenstein model.....	25
<b>3.3 Control of the Fermi energy level of an Insulated-gate thin-film tin dioxide transistor having a multigate structure .....</b>	<b>29</b>
<b>4. TECHNOLOGY – EXPERIMENTAL.....</b>	<b>31</b>
<b>4.1 Transistor technologies .....</b>	<b>31</b>
4.1.1 Definitions .....	31
4.1.2 FET-based semiconductor gas sensors .....	31
<b>4.3 Technology – Buried gates .....</b>	<b>33</b>
<b>4.4 Experimental – platinum electrodes and gas sensitive material.....</b>	<b>34</b>
4.4.1 Deposition of platinum.....	34
4.4.2 Deposition of gas sensitive material.....	37
4.4.3 Results of backend process.....	39
<b>5. EXPERIMENTAL – GATE VOLTAGE PULSED OPERATION / TEMPERATURE CONTROL.....</b>	<b>41</b>
<b>5.1 Control of gate voltages .....</b>	<b>41</b>
5.1.1 Specification.....	42

5.1.2	Realisation of pulse .....	44
5.1.3	Realisation of output stages .....	45
5.1.4	Realisation of power supply .....	46
<b>5.2</b>	<b>Control of operation temperature.....</b>	<b>49</b>
<b>6.</b>	<b>MEASUREMENTS AND CONCLUSIONS .....</b>	<b>55</b>
6.1	Source-drain characteristics of the Insulated-gate TFT.....	55
6.2	Gas measurement proceedings .....	57
6.3	Gas measurement.....	58
6.3.1	Sensor response to hydrogen.....	58
6.3.2	Sensor response to carbon monoxide .....	62
6.3.3	Sensor response to nitrogen dioxide .....	64
6.3	Summary and Conclusions.....	66
<b>7.</b>	<b>OUTLOOK .....</b>	<b>67</b>
	<b>APPENDIX A - User manual for gate voltage/temperature pulsed operation.....</b>	<b>69</b>
	<b>APPENDIX B – Protocol for backend process.....</b>	<b>71</b>
	<b>APPENDIX C – Gas Measurement.....</b>	<b>77</b>
	<b>REFERENCES .....</b>	<b>79</b>

## FIGURE REGISTER

Page no.	Description
5	2.1. Parts of a MOSFET
6	2.2. Electron energy bands of a doped semiconductor
9	2.3. Electric field across oxide-semiconductor interface
10	2.4. Voltage drop across oxide-semiconductor interface
11	2.5. Cross section of a MOSFET in inversion operation
12	2.6. Electron energy level gradients for a semiconductor in electric field
13	2.7. Electron energy levels along the channel for an n-type MOSFET
16	3.1. TFT characteristics
17	3.2. Electron energy levels of SnO <sub>2</sub>
19	3.3. Oxygen concentration dependency for SnO <sub>2</sub>
20	3.4. Bending of energy levels in SnO <sub>2</sub> for chemisorption
23	3.5. Low power semiconductor gas sensor
24	3.6. Transistor layout of SnO <sub>2</sub> MOSFET
25	3.7. Gate voltage pulsed operation
26	3.8. Energy diagram of chemisorbed adatoms
27	3.9. Chemisorption of O <sub>2</sub> <sup>-</sup> on thin ZnO film
30	3.10. Illustration of control of Fermi energy gradient
32	4.1. Sensor layout
33	4.2. Scanning electron microscope image of gate electrodes
35	4.3. Deposition of aluminium as sacrificial layer
35	4.4. Aluminium wet etching
36	4.5. Deposition of tantalum/platinum
37	4.6. Tetragonal crystal structure of tin dioxide
38	4.7. Illustration of WO <sub>3</sub> - structure
39	4.8. Scanning electron microscope images of the sensor
40	4.9. Scanning electron microscope images of the metal oxide grains
41	5.1. Construction of gate voltage pulsed operation
42	5.2. Specifications of gate voltage pulsed operation
42	5.3. Outputs of gate voltage pulsed operation
43	5.4. Measurement set up
44	5.5. Realisation of pulse
45	5.6. Realisation of output stages for GVPO
45	5.7. Realisation of output stages for temperature pulsed operation
46	5.8. Realisation of power supply
47	5.9. Calculations of full-wave rectified signal
49	5.10. Circuit diagram of temperature controller
51	5.11. Gate signal response for regulated temperature
52	5.12. Step response for regulated temperature

56	6.1. Experimental drain characteristic of an SnO <sub>2</sub> based IGFET TFT
59	6.2. Sensor response to hydrogen at ~200°C
60	6.3. Sensitivity variations to hydrogen at ~200°C
61	6.4. Sensor response for operation temperature at ~280°C
62	6.5. Sensor response to carbon monoxide at ~200°C
63	6.6. Sensitivity variations to carbon monoxide at ~200°C
64	6.7. Sensor response to nitrogen dioxide at ~200°C
65	6.8. Sensitivity variations to nitrogen dioxide at ~200°C

### 1. Introduction

In this final thesis a semiconductor gas sensor for detection of reducing gases (e.g. carbon monoxide) and oxidising gases (e.g. nitrogen dioxide) is analysed. The development of the sensor is a co-operation with Micronas and Fraunhofer Institute for Physical Measurement Techniques (Fraunhofer IPM). Simulations and calculations of the sensor performance are being performed at Technical University of Illmenau.

Micronas is a world-wide producer of application specific chip solutions for commercial electronics, multimedia and automotive electronics. The holding is headquartered in Zurich. Freiburg is a location for both development and production of cutting-edge ICs and sensor system solutions. The Fraunhofer co-operation is spread all around Germany and performs research in all fields of engineering. Fraunhofer IPM is one of Freiburg's five Fraunhofer institutes.

A semiconductor gas sensor can be used within applications like:

- Monitoring of dangerous/hazardous gases
- Automotive/Aerospace industry
- Environmental technologies

A gas sensor has to be able to detect very small amount of gases in the ambient atmosphere when used as an air quality device or used within process measurement technology. A semiconductor gas sensor can detect gases from concentrations in magnitude of parts per million (ppm) (in case of NO<sub>2</sub> or ozone ppb) in the atmosphere. The size of a semiconductor gas sensor element can be very small, which in this context means a few square micrometers ( $\mu\text{m}^2$ ).

The main requirements for semiconductor gas sensors are:

- Long term stability
- Low costs
- Small size
- Good resolution
- Controllability of gas sensitivity
- High cross-sensitivity to gases
- Low power consumption

There exist a wide range of different technologies used for semiconductor gas sensors at the market and in the research area. There are also alternative gas detection methods, for instance spectrometric sensors and electro-chemical cells. Different trade-offs of

## 1. Introduction

---

the performance of a gas sensor must always be considered depending on its applications and the budget.

For measurements of harmful substances in the air in ppb- and ppm-range resistive semiconductor gas sensors have been advancing the last years. The benefits of these sensors are, mainly, the cost-effective fabrication, combined with possibilities for system-on-chip solutions for processing of the measurements. Semiconductor gas sensors are electrical sensors, whose conductivity changes by influences of gases at temperatures between 50 and 900°C. Typical detection gases are NO<sub>x</sub>, CO, hydrocarbon, NH<sub>3</sub>, O<sub>3</sub> and H<sub>2</sub>O. As gas sensitive elements different metal oxides (e.g. SnO<sub>2</sub>, WO<sub>3</sub>, Ga<sub>2</sub>O<sub>3</sub>, Cr<sub>2-x</sub>Ti<sub>x</sub>O<sub>3</sub> etc.) are possible to use. These are implemented using thick-film or thin-film techniques. Further, a structure for a heater electrode is integrated onto the chip to achieve a desirable operation temperature. The detection of gases is accomplished due to adsorption and desorption of gases. The adsorption and desorption probabilities of different gases are commonly controlled by the operation temperature. However, the developed and characterised sensor within the scope of this final thesis affects the adsorption probability by the field effect. This electric adsorption effect was postulated by Fedor Wolkenstein 1957. This effect arises the possibility to operate a gas sensor at relatively low temperatures and, thereby, be able to integrate CMOS electronics at the same chip.

The final thesis has been performed at Fraunhofer IPM. The assignment was to investigate the prospects of a semiconductor MOSFET gas sensor and in particular the performance of such a gas sensor at low temperatures. The experimental part of the final thesis comprises:

- Thin-film deposition of source/drain contacts and heating electrodes, all in platinum.
- Thin-film deposition of the gas sensitive material, SnO<sub>2</sub>/WO<sub>3</sub>.
- Design and implementation of a measurement system for control of gate potentials.
- Design of a operation temperature controller for platinum electrodes.
- Evaluations of the sensor's characteristics and performance.
- And finally evaluation of the obtained results.

## 1. Introduction

---

The report is divided into these chapters.

### **Chapter 2**

This chapter describes the functionality of a Metal-Oxide-Semiconductor field effect transistor. Important terms as doping, Fermi-Dirac distribution and field effect for MOSFETs found in ICs, and for thin-film transistor gas sensors as well, are introduced.

### **Chapter 3**

How thin-films of metal oxides can be used as gas sensitive elements is presented in this chapter. The gas sensitive properties are described according to the Wolkenstein model for thin-films of metal oxides.

### **Chapter 4**

This chapter comprises the experimental part for the sensor technology. Basically, the technology for gates and insulator layer has been performed by Micronas. The technology for source/drain contacts and heating electrodes and gas sensitive material has been performed at Fraunhofer IPM and is an experimental part of this final thesis.

### **Chapter 5**

This chapter is about design and implementations of a measurement system for control of gate potentials and a design of a operation temperature controller using one on-chip platinum electrode.

### **Chapter 6**

Measurements and conclusions.

### **Chapter 7**

A chapter about future work and extensions finishes the report.

**1. Introduction**

---

## 2. Theoretical description of a Metal-Oxide-Semiconductor field effect transistor

### 2. Theory of a Metal-Oxide-Semiconductor field effect transistor

The first section of this chapter describes the functionality of a **Metal-Oxide-Semiconductor field effect transistor**, commonly denoted MOSFET. The second section is about how the behaviour of a MOSFET can be explained with basic semiconductor physics. The purpose of this chapter is to introduce fundamental concepts within semiconductor electronics and to give a basic understanding of how a MOSFET operates.

#### 2.1 Introduction

The term Metal-Oxide-Semiconductor describes the different layers of a MOSFET. The gate is a metal contact (in commercial devices today mainly polycrystalline silicon). Next to the gate there is an oxide insulator. At the opposite side of the insulator there is a semiconductor. The semiconductor can be described as a material which can act both as an insulator and a conductor. All different kinds of MOSFET devices consist of a source, drain and gate electrode. The source provides charge carriers and the drain collects charge carriers. For an n-type MOSFET the charge carriers are negative electrons. For a p-type MOSFET the charge carriers are positively charged holes.

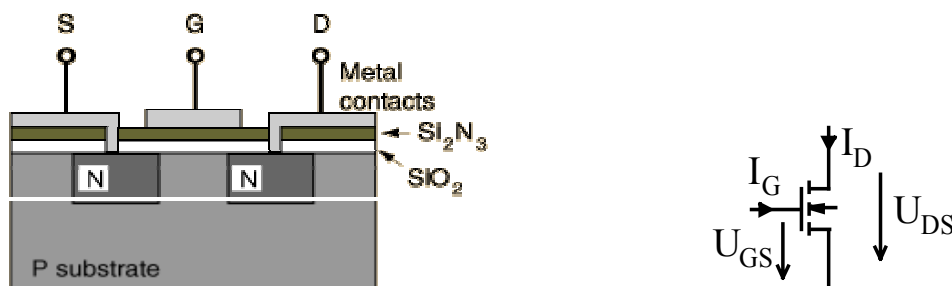


Figure 2.1. On the left: Main parts of an n-type MOSFET (URL - hyperphysics). The source and drain, for this MOSFET configuration, are two n-doped semiconductor regions. The gate is separated from the p-substrate by an insulating dielectric layer. On the right: Circuit symbol for an n-type MOSFET with enhancement-mode. An n-type MOSFET with enhancement-mode requires a voltage potential over gate and source that is raised over a positive threshold voltage potential in order to conduct current across source and drain.

The amount of current from source to drain can be controlled by establishing an electric field in the semiconductor, capacitively coupled through a dielectric layer, in the direction traverse to the current flow. The voltage potential across source and gate,  $V_{GS}$ , is used as a size of the established "connection" between source and drain. A MOSFET can be seen as a switch, either used for logical functions or to provide current and voltage gain in electronic circuits.

## 2. Theoretical description of a Metal-Oxide-Semiconductor field effect transistor

### 2.2 Physical description of a MOSFET

#### 2.2.1 Doping of semiconductors

The electrical conductivity properties of a semiconductor arise by adding specific impurities to the material. For classical semiconductors, like silicon (Si), germanium (Ge), gallium-arsenide (GaAs) or zinc-selenide (ZnSe) (Larsson-Edefors, 2000), the impurities either have one more or one less valence electron than what the pure material has. For semiconducting metal oxides, however, the doping mechanism can be explained by oxygen vacancies or oxygen surpluses in the lattice structure. The doping of semiconductors for standard ICs and semiconducting metal oxides have similarities. An impurity atom, which has one extra valence electron (donor atom), contributes with a potential conduction electron. Loosely bound electrons to the positive metal ion of a oxygen vacancy in a metal oxide are potential conduction electrons as well. An impurity atom, which has one less valence electron than what the pure material has (acceptor atom), contributes with a potential conduction hole. A hole is created when a molecule binding of an acceptor and semiconductor atom borrows an electron to create a covalent bond. Loosely bound holes to the positive metal ion of an oxygen surplus in a metal oxide are potential conduction holes as well. In conclusion, important properties like electron drift, Fermi-Dirac distribution, Poisson's equation and Debye-length, which all are essential parameters for the characteristics of a MOSFET, can modulate the bulk properties of a MOSFET gas sensor. The remaining part of this chapter discusses these fundamental topics.

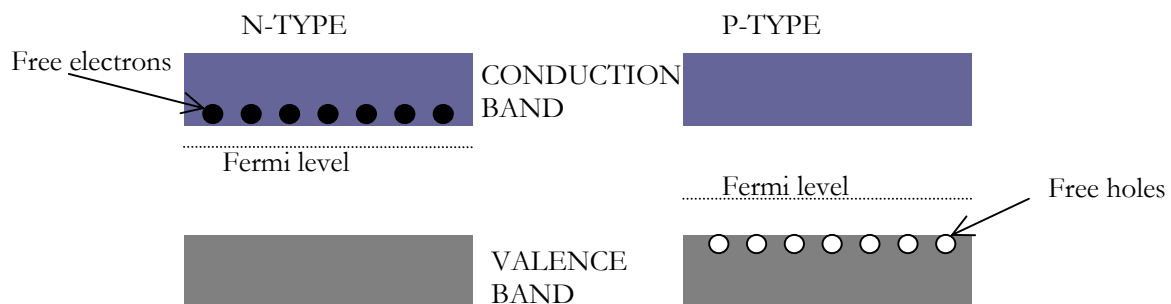


Figure 2.2. Electron energy bands of a semiconductor . These can be seen as continuous due to interatomic forces in a material (Per Larsson-Edefors, 2000).

## 2. Theoretical description of a Metal-Oxide-Semiconductor field effect transistor

### 2.2.2 Equilibrium state of a semiconductor

The Fermi energy level is the energy level for which the Fermi-Dirac distribution function is equal to  $1/2$ . The Fermi-Dirac distribution function for an electron tells how big the probability is that a certain electron energy level is occupied.

Fermi-Dirac distribution function:

$$f(E) = \frac{1}{1 + e^{\frac{(E-E_F)}{kT}}} \quad (1)$$

The Fermi-Dirac distribution function is only valid in equilibrium state. In non-equilibrium state the electron distribution is described by quasi-Fermi levels. A region in a uniformed semiconductor is in equilibrium state when it is charge neutral, that is

$$p_0 - n_0 + N_d - N_a = 0 \quad (2)$$

$p_0$  and  $n_0$  is the carrier concentration of holes and electrons respectively.  $N_d$  and  $N_a$  are the number of positive and negative ions, caused by doping, respectively.

For a non-uniformed semiconductor an internal electric field compensates for the gradient in doping profile. For an equilibrium state in a non-uniformed semiconductor to hold Einstein's relationship must be fulfilled (Larsson-Edefors, 2000), that is

$$J_{n,x} = J_{n,drift} + J_{n,diffusion} = nq\mu_n E_x + qD_n \frac{dn}{dx} = 0 \quad (3)$$

$J_{n,x}$ : current density of free electrons in one direction (x).

$n$ : doping concentration of electrons.

$q$ : electron charge.

$\mu_n$ : mobility of electrons.

$E_x$ : electric field in one direction (x).

$D_n$ : diffusion coefficient.

$dn/dx$ : doping gradient of donors in one direction (x).

The electron mobility is defined as

$$\mu_n = \frac{qt_{cn}}{m_n^*} \quad (4)$$

$t_{cn}$ : mean free time - probability that a electron collide within the time dt is dt/  $t_{cn}$ .

$m_n^*$ : conductivity effective mass of an electron.

## 2. Theoretical description of a Metal-Oxide-Semiconductor field effect transistor

Larger values of  $\tau_{cn}$  lead to increased mobility for electrons. However, electrons do not accelerate to infinite velocity by exposure to an electric field, but will reach a saturation speed. Equation (4) is only realistic for electron velocities below the saturation velocity.

The diffusion coefficient is defined as

$$D_n = kT \frac{t_{cn}}{m_n^*} \quad (5)$$

$k$ : the Boltzmann constant.

$T$ : absolute temperature.

The first term in equation (3),  $J_{n,drift}$ , is due to the fact that electrons want to move in the direction towards a lower energy state. The phenomena is called drift.

The second term in equation (3),  $J_{n,diffusion}$ , is due to random thermal motion of electrons (Per Larsson-Edefors, 2000). The phenomena is called diffusion.

The relationship in equation (3) must also hold for holes at equilibrium in a non-uniformed semiconductor (Larsson-Edefors, 2000), that is

$$J_{p,x} = pq\mu_p E_x + qD_p \frac{dp}{dx} = 0 \quad (6)$$

$$\mu_p = \frac{qt_{cp}}{m_p^*} \quad (7)$$

$$D_p = kT \frac{t_{cp}}{m_p^*} \quad (8)$$

## 2. Theoretical description of a Metal-Oxide-Semiconductor field effect transistor

### 2.2.3 N-channel of an n-type MOSFET

A MOSFET has three defined operation states, accumulation, depletion and inversion. When a positive electric field is present in the direction towards the gate the transistor is in accumulation operation (n-type transistor). Depletion operation is established when the electric field is positioned in the opposite direction. When the voltage drop across the depletion region, a contact potential across two regions with different electron energy distributions, is saturated the transistor enters inversion operation. A model of the static behaviour of the voltage drop across a depletion region can be extracted by using Poisson's law (Grant, Gowar, 1989):

$$\begin{aligned} \frac{d^2V}{dx^2} &= \frac{qN_A}{\epsilon_o\epsilon_{si}}, & 0 \leq x \leq l_p \\ \frac{dV(l_p)}{dx} &= 0 \\ V(x) &= \frac{qN_A}{2\epsilon_o\epsilon_{si}}(l_p - x)^2, & 0 \leq x \leq l_p \quad (9) \end{aligned}$$

$l_p$ : depletion region length.

$qN_A$ : charge density.

$\epsilon_o$ : relative permittivity of vacuum.

$\epsilon_{si}$ : relative permittivity of silicon.

This model assumes that the substrate has a uniform cross-sectional area and that all material in the substrate is either in depletion or inversion state.

Figure 2.3 illustrates the electric field of the oxide-semiconductor interface in depletion operation.

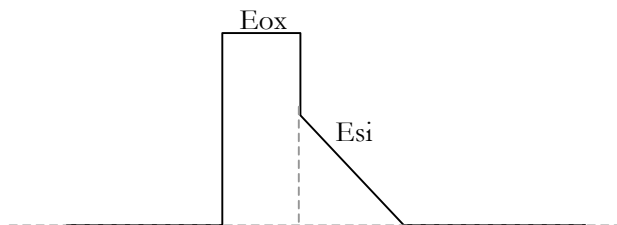


Figure 2.3. Electric field in direction from the positive charge density  $Q$  at the gate to the substrate, in this case silicon.  $E_{OX}$ : electric field through the oxide.  $E_{Si}$ : electric field through the depletion region of doped silicon.

## 2. Theoretical description of a Metal-Oxide-Semiconductor field effect transistor

The discontinuity of this electric field at the insulator-semiconductor interface is due to impurities that always are present. The positive impurity charge density, denoted  $Q_{SS}$ , is:

$$Q_{SS} = \epsilon_o \epsilon_{ox} E_{OX} - \epsilon_o \epsilon_{si} E_{Si} (x = 0) \quad (10)$$

The voltage drop across the entire oxide-semiconductor interface is equal to the applied voltage potential.

$$V_{GB} + V_{CP} = V_{OX} + \Delta V \quad (11)$$

$V_{GB}$  : gate potential.

$V_{CP}$  : contact potential.

$V_{OX}$  : voltage drop across the oxide.

$\Delta V$  : voltage drop across the depletion layer.

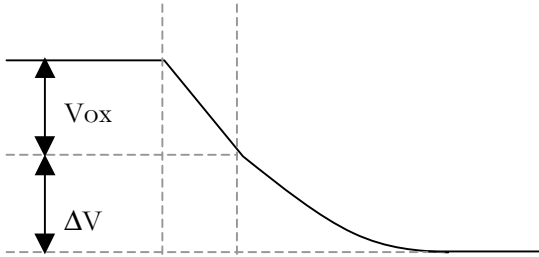


Figure 2.4. Voltage drop across an oxide-semiconductor interface (Grant, Gowar, 1989). The voltage drop  $\Delta V$  is illustrated according to expression (9).

An increase of  $V_{GB}$  causes an increase of  $V_{OX}$  and  $\Delta V$ . However,  $\Delta V$  will be saturated at a certain point,  $\Delta V_{TH}$ . For this simple model, when  $V_{GB}$  increases further only the voltage across the oxide,  $V_{OX}$ , will increase. This is caused not only by the increased positive charge density at the gate-oxide interface, but also by a thin substrate layer containing free electrons, called n-channel, at the oxide-semiconductor interface.

## 2. Theoretical description of a Metal-Oxide-Semiconductor field effect transistor

### 2.2.4 Potential variation from gate to substrate of an n-type MOSFET influenced by an electric field

For the assumptions that:

- no electric field exists parallel to the gate-oxide-substrate interface,
- the impurity charge density,  $Q_{ss}$ , is equally distributed along the oxide-semiconductor,
- The substrate next to the insulator is either in depletion or inversion state,

the charge distribution of the n-channel can be illustrated according to figure 2.5.

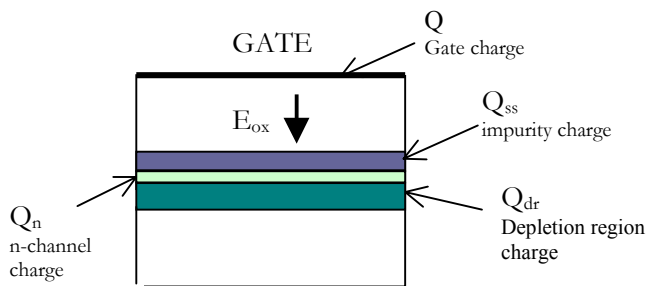


Figure 2.5. Cross section of a MOSFET in inversion operation (Larsson-Edefors, 2000).

The implication of the statements above is that the mobile electronic charge per unit area in the inversion layer,  $Q_n$ , increases linearly with  $V_{GB}$  above the threshold voltage (Grant, Gowar, 1989). However, in reality a smooth junction from inversion to depletion region is formed. Since the semiconductor enters a non-equilibrium state with an applied gate charge,  $Q$ , charge-neutrality is not fulfilled:

$$p_0 - n_0 + N_d - N_a \neq 0$$

where  $p_0$  and  $n_0$  vary exponentially with the local Fermi level. A more rigorous relation for the potential variation as a function of vertical depth, which includes this fact, in a uniform doped semiconductor is (Grant, Gowar, 1989):

$$\frac{d^2\psi}{dX^2} = K \sinh \psi + 1 \quad (12)$$

$$\psi = qV_i / kT$$

$V_i$ : mid band potential.

$X$ : normalised length.

$K$ : constant.

## 2. Theoretical description of a Metal-Oxide-Semiconductor field effect transistor

### 2.2.5 Potential variation from source to drain of an n-type MOSFET influenced by an electric field

The electrons are not only influenced by an electric field from gate to substrate, but also an electric field from drain to source when they are at different voltage potentials. The implication of this is that the energy levels  $E_c$  (conduction energy level),  $E_v$  (valence band energy) and  $E_i$  (mid band energy) will have a non-zero gradient over the voltage drop from drain to source.

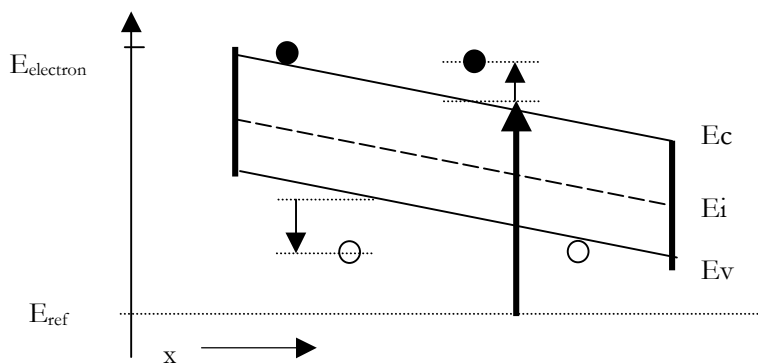


Figure 2.6. Illustration of electron energy level gradients for a semiconductor (Larsson-Edefors, 2000). The right end is applied to + and the left end is applied to ground for this piece of semiconductor. The thick arrow represents potential energy and the two thin arrows represent kinetic energies. The figure illustrates the motion of both free electrons and free holes.

How the electron energy levels are affected for an n-type MOSFET, having n-doped source and drain contacts, at the oxide-semiconductor interface at different operation regions are basically illustrated in figure 2.7. The thin lines represent electron energy levels at zero gate voltage and the thick lines represent electron energy levels at the specific operation points, that is when a positive gate voltage potential is applied. For all three operation points the source is connected to ground, which explains why the Fermi level and conduction level of the source coincide (the arsenal of electrons at the negative pole). Operation point A corresponds to a fully turned on transistor. The ohmic voltage drop along the channel can be seen at the gradient of the Fermi level. In operation point B the transistor is operating at a region with constant current, often called saturation region. Here the substrate only remains inverted outside the influence of the drain voltage potential. Finally, operation point C represents a transistor that is turned off.

## 2. Theoretical description of a Metal-Oxide-Semiconductor field effect transistor

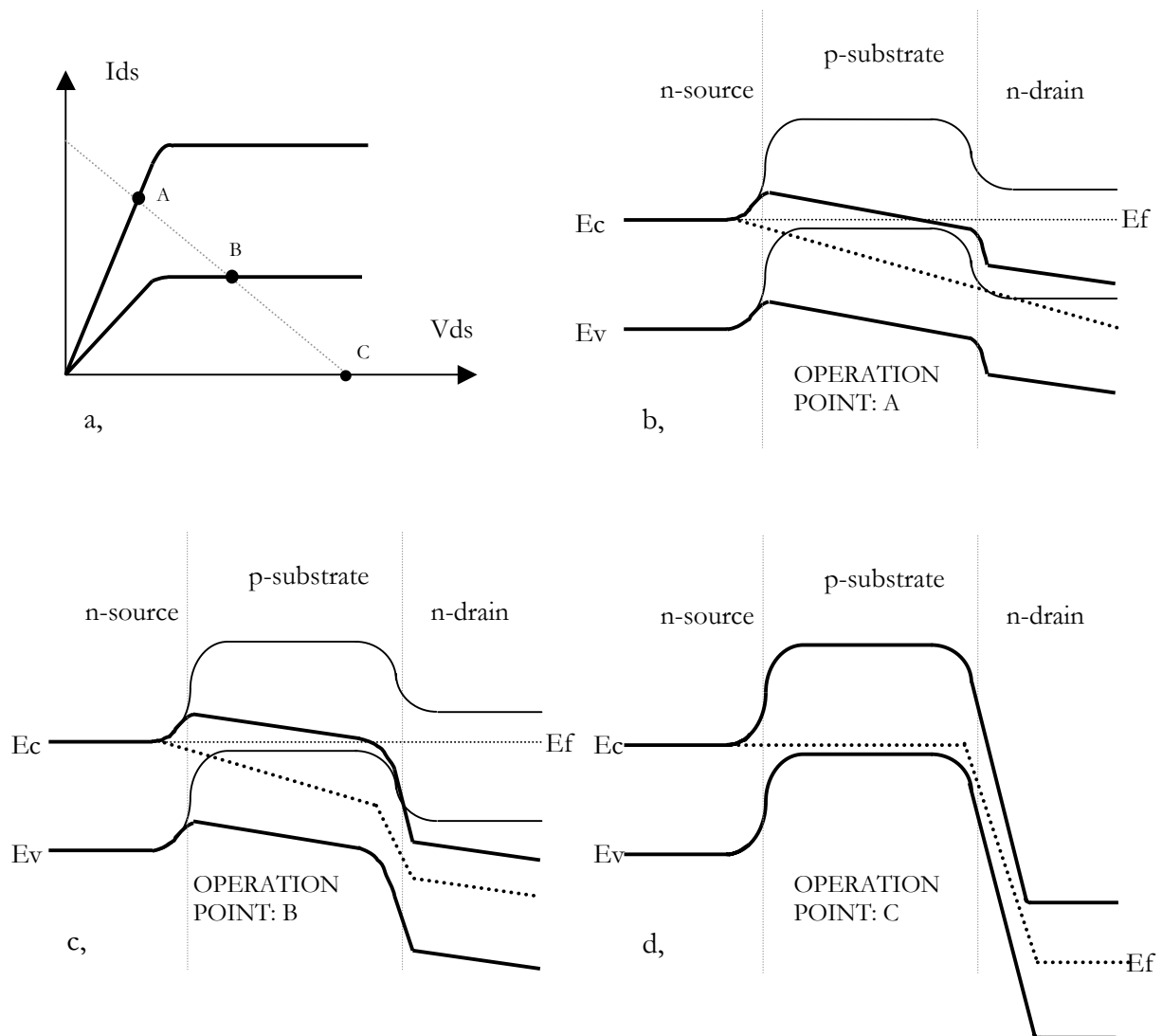


Figure 2.7. Illustration of electron energy levels along the channel for an n-type MOSFET at different operation points (Grant, Gowar, 1989). a, Characteristics of the transistor. b,-c,-d, Electron energy levels corresponding to operation point A, B and C in figure (a), respectively. The thin lines, in figure b and c, represent the operation points for  $V_{GS}=0$ . The thick lines represent an applied positive gate voltage,  $V_{GS}>0$ . The dotted lines are Fermi levels.

The current flow in an n-type MOSFET is due to electrons ability to drift. The drift mechanism causes electrons to move from a higher energy level to a lower. The illustrations in figure 2.7 indicates that it is the conduction energy level,  $E_c$ , in the leftmost part of the n-channel that decides the threshold voltage. As soon as the electrons have managed to pass this "barrier" they will continue to drift towards drain.

## **2. Theoretical description of a Metal-Oxide-Semiconductor field effect transistor**

The drain voltage counteracts the electric field from the gate. This surface effect results in the pinched-off effect, a sort of saturation mechanism. Different layouts are used, especially for power MOSFETs, to modulate the channel behaviour. The MOSFET gas sensor, which is the focus of this work, has a TFT structure, that is source and drain are metal contacts. The idea is to modulate the channel behaviour of this sensor by a multigate structure. The gates of this transistor are buried below an insulator.

### 3. Gas sensing properties of an Insulated-gate thin-film tin dioxide transistor

## 3. Gas sensing properties of an Insulated-gate thin-film tin dioxide transistor

The first section of this chapter describes the functionality of a thin-film transistor (TFT) and the gas sensing properties of tin dioxide. The second section is about how the gas sensing properties of tin dioxide can be affected. This section is mainly focusing on control by external electric field for an Insulated-gate thin-film transistor. The third section motivates the idea of a MOSFET gas sensor with multigate structure.

### 3.1 Gas sensing properties of tin dioxide

#### 3.1.1. Definition of thin-film transistor

Modern electronics can be produced in a very small size. Thin-film technology makes this possible. Not only are the electronics made small with this technology, but also fast, effective and cost-effective. A thin-film transistor (TFT) is a transistor whose semiconducting channel is a thin-film. Even though modern integrated circuits are made in thin-film technology there are no TFTs. These transistors are made on silicon wafers, or other potential semiconductors, and use the top layer of the silicon substrate, the bulk, as semiconductor, which is achieved by a doping process. The other parts of the transistors are made in thin-film technology, though. Thin-film transistors are, for instance, found in LCD-displays where they are used to control individual picture elements. For this application a semiconducting thin-film is deposited onto a transparent insulator.

To conclude this section one can define a gas sensitive thin-film tin dioxide transistor as a transistor whose semiconductor is a thin-film of tin dioxide ( $\text{SnO}_2$ ). The gas sensitive properties arise by different types of chemisorptions, according to the Wolkenstein model (section 3.2.3 *Wolkenstein model*). Chemisorption occur when the sensor chemically interacts with gas molecules, so-called adatoms.

#### 3.1.2 Characteristics of Insulated-gate thin-film transistors

The primary operating mechanism of an Insulated-gate thin-film transistor, the TFT, is conductivity modulation of the channel by field effect. A simple model of a TFT, which predicts the drain characteristics expected solely from the effect of electric fields produced by the potentials applied to the electrodes, is (H.Borkan, K.Weimer.P):

### 3. Gas sensing properties of an Insulated-gate thin-film tin dioxide transistor

$$I_d = \frac{\mu C_g}{L^2} \cdot (V_g - V_0) V_d - \frac{\mu C_g}{L^2} \frac{V_d^2}{2}$$

$I_d$ : drain current.

$\mu$ : electron mobility.

$C_g$ : gate capacitance.

$L$ : channel length.

$V_g$ : gate potential.

$V_0$ : threshold potential.

$V_d$ : drain potential.

For this model the potential of the semiconductor at an arbitrary point  $x$ ,  $V(x)$ , varies linearly between source and drain.

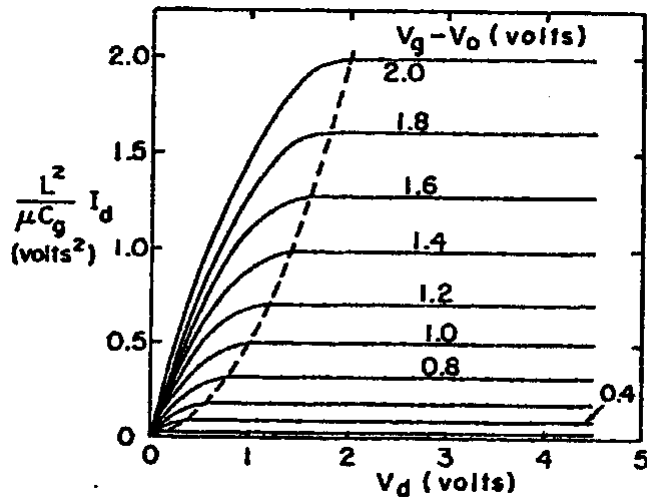


Figure 3.1. Theoretically predicted TFT drain characteristics. The dashed line is the locus of the knees of the curves. The model is valid up to the points where the slope is zero, that is up to the saturation region. There is a square-law relationship of saturated drain current with the effective gate voltage. These predictions have been proven to be good in comparison with experimental data for TFTs.

#### 3.1.3 Semiconductor properties of tin dioxide

Pure tin dioxide is an insulator. Its band gap is  $\sim 3.6$  eV, which can be compared to silicon's  $\sim 1.1$  eV. The structure of pure tin dioxide consists of a lattice of tin atoms,  $\text{Sn}^{4+}$ , and oxygen atoms,  $\text{O}^{2-}$ . The most interesting property of tin dioxide, and other conceivable metal oxides used for semiconductor gas sensors, is oxygen vacancies in

### 3. Gas sensing properties of an Insulated-gate thin-film tin dioxide transistor

the crystal structure (or surpluses for p-type metal oxides), whose concentration depends on temperature and gas composition at the surface. The process where a concentration increase of oxygen vacancies is achieved by heating is called annealing and can be compared to doping of semiconductors like silicon or germanium. Loosely bound electrons of the vacancies have a very high probability, in comparison to valence electrons, to reach the conduction band and thereby contribute to conductivity properties of the material. N-type tin dioxide is often denoted  $\text{SnO}_{2-x}$ .

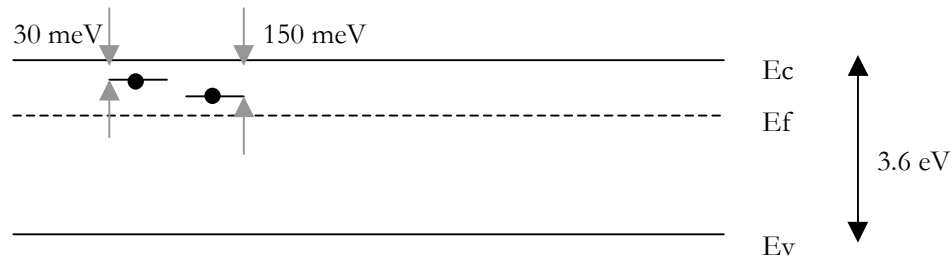


Figure 3.2. Electron energy diagram of  $\text{SnO}_{2-x}$  (band gap : 3.6 eV). When an oxygen vacancy is formed, a neutral oxygen atom is released and two electrons of the oxygen ion remain loosely bound to the oxygen vacancy. The two established donor levels are shown in the figure,  $E_{01}=30$  meV (single ionisation) and  $E_{02}=150$  meV (double ionisation). (W.Hellmich, T.Doll etc.).

This chapter is mainly focusing on tin dioxide. However, the theory presented also holds for other semiconducting n-type metal oxides (e.g. ZnO,  $\text{TiO}_2$ ,  $\text{Ga}_2\text{O}_3$ ,  $\text{V}_2\text{O}_5$ ,  $\text{WO}_3$ ).

#### 3.1.4 Nitrogen oxides and carbon monoxide

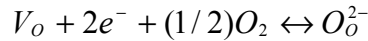
Nitric oxide (NO) and nitrogen dioxide ( $\text{NO}_2$ ) are often named  $\text{NO}_x$  or nitrogen oxides. These compounds are formed by the oxidation of atmospheric nitrogen under high-energy conditions (Internationella Miljöinstitutet Lund, Sweden). At high temperatures or by exposure to ultraviolet light nitrogen dioxide ( $\text{NO}_2$ ) molecules are spontaneously broken down into nitric oxide (NO).  $\text{NO}_x$  contributes to acidification and decomposition of buildings.  $\text{NO}_x$  is a form of pollution often associated with diesel engines. Carbon monoxide (CO) is a product of incomplete burning of hydrocarbon-based fuels. Cars are by far the biggest contributor to carbon monoxide pollution in industrialised countries (U.S. Environmental Protection Agency). Both nitrogen oxides and carbon monoxide might harm the heart and blood vessels. Higher concentrations are found in urban and industrial areas.

### 3. Gas sensing properties of an Insulated-gate thin-film tin dioxide transistor

#### 3.1.5 Principles of nitrogen oxides and carbon monoxide measurement

Tin dioxide deposited by electron-beam, reactive sputtering or thermal evaporation exhibit a polycrystalline structure. A polycrystalline semiconductor has a structure with grains, which by the contact areas to other grains can conduct current. In contrast to singlecrystalline materials, polycrystalline materials give rise to local potential barriers, which arise between the grains. The electric properties at the surface of the thin-film and the surface boundaries of the grains are affected by the adsorption and desorption of gas molecules. One can distinguish between two sorts of adsorption phenomena; physisorption and chemisorption. Physisorption is caused by Van-der-Waals forces, which are forces of electrostatic nature. Chemisorption is based on stronger covalent forces (H.Geistlinger, 1993). The mechanism when the bond of an adatom is released is called desorption.

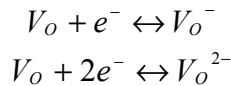
There is a chemical balance between oxygen ions bound by chemisorption and physisorption at the tin dioxide boundaries. This interaction is an elementary reaction for semiconductor gas sensors. The thermally generated vacancies of the material boundary interact with adsorbed atmospheric oxygen via the reversible reaction (W.Hellmich, T. Doll, etc., 1997):



$V_o$  : a neutral vacancy that has released its two loosely bound electrons ( $e^-$ ) to the conduction band.

$O_o^{2-}$  : two-fold charged oxygen ion on a normal oxygen site in the  $SnO_2$  network.

Neutral vacancies within the grains can interact with electrons in the conduction band (W.Hellmich, T.Doll, etc., 1997):



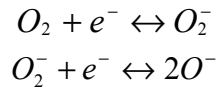
$V_o^-$  : single charged oxygen vacancy.

$V_o^{2-}$  : double charged oxygen vacancy.

The equilibrium state of these reactions is dependent on the local Fermi level. The local "doping" level across the bulk has to fulfil charge neutrality. The balance of neutral vacancies and two-fold charged oxygen ion suggests an interaction with atmospheric oxygen and electrons in the conduction band.

### 3. Gas sensing properties of an Insulated-gate thin-film tin dioxide transistor

Oxygen ions can be found at the material boundaries. Already at room temperature  $O_2$  is chemisorbed to  $O_2^-$ . A chemisorption by gaining one further electron from the surface is observed for temperatures above  $150^\circ\text{C}$  and is the dominating chemisorbed state for oxygen at the metal oxide surface above  $400^\circ\text{C}$ .



These ions can be modelled as an external field near the material boundaries. This effect is shown in figure 3.4. and has a great influence on the conductivity of a thin-film of metal oxide.

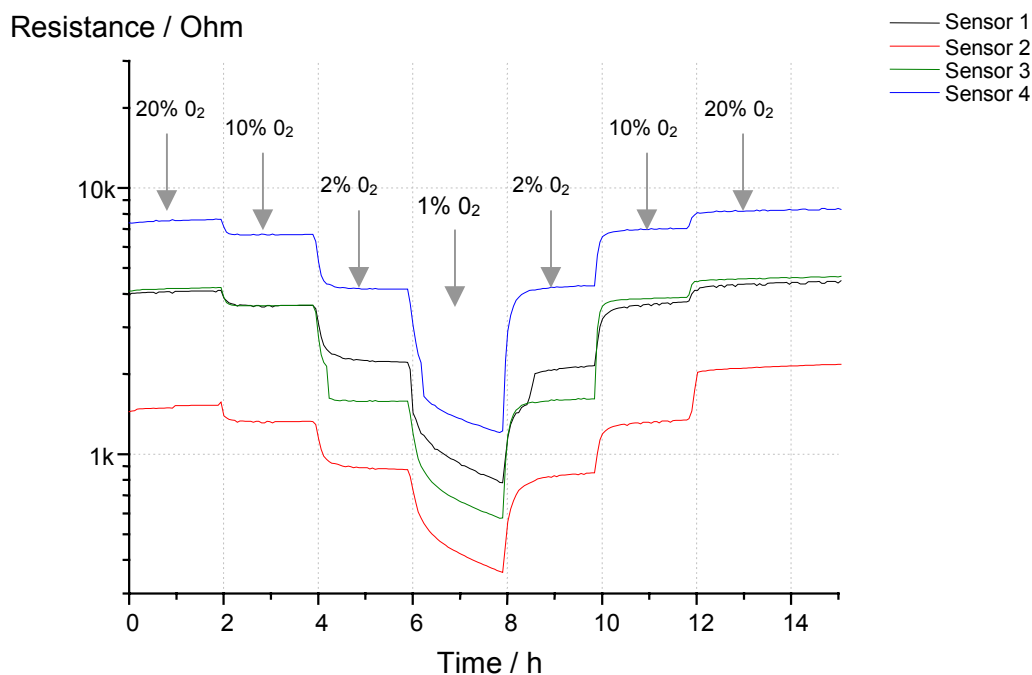
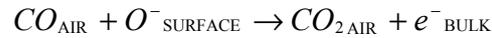


Figure 3.3. Resistance measurement of a thin-film of tin dioxide, four different sensors, at approximately  $400^\circ\text{C}$  for different oxygen concentrations in  $N_2$ . The measurement has been performed in IPM's gas laboratory. The deposition technology for these layers and the one used for the MOSFET gas sensors analysed in this work are the same.

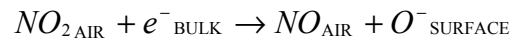
### 3. Gas sensing properties of an Insulated-gate thin-film tin dioxide transistor

Carbon monoxide (CO) molecules react with chemisorbed oxygen at the material boundaries:



A negative charge carrier is added to the bulk and the coverage of chemisorbed oxygen ( $O_2^-$ ,  $O^-$ ) at the material boundaries decreases. Hence, the resistance decreases.

Nitrogen dioxide ( $NO_2$ ) molecules take conducting electrons from the material:



Thereby a concentration increase of chemisorbed oxygen ( $O_2^-$ ,  $O^-$ ) at the material boundaries occurs. These two effects will cause the resistance to increase.

Since nitric oxide becomes nitrogen dioxide relatively fast at temperatures below 200°C, it also contributes to the gas reactions. The sensitivity of nitrogen dioxide is, consequently, combined with nitric oxide;  $NO/NO_2$  - sensitivity.

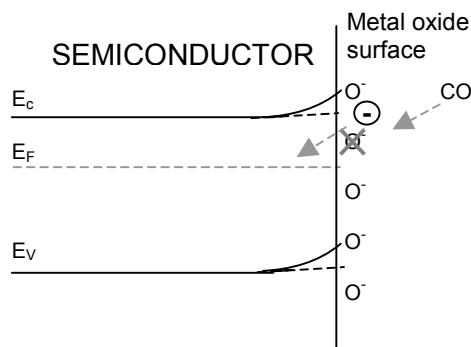


Figure 3.4. Illustration of change in energy band diagram caused by chemisorption of CO. A negative charge carrier is injected into the semiconductor ( $E_C$ ,  $E_F$  and  $E_V$  are energy levels of the bulk) and the coverage of chemisorbed oxygen at the surface decreases. The curved shape of the energy levels, caused by physisorption, is straightened by this reaction (dashed curves) and the conductivity increases. The effect is most noticeable within the Debye-length of the bulk.  $NO_2$  has the opposite effect. In order to have a high gas sensitivity (large conductivity change) the thin-film thickness should be in order of the Debye-length (the screening length). This view assumes that the chemisorption, which influences the charge carrier concentrations, occurs at the surface of the thin-film.

### **3. Gas sensing properties of an Insulated-gate thin-film tin dioxide transistor**

The size of the grains play an important role for the conducting properties of the thin-film. For large grain sizes, that is when half the grain size is larger than the Debye-length the change of the potential barriers at the contact areas between the grains dominates. This situation is typical for thick-film techniques. For thin-films with typical grain sizes from few nm up to 100 nm and Debye-length from few nm up to some 100 nm the modulation of charge carriers by gas reactions can be analysed by alterations of the conduction level (figure 3.4). Using this view it is obvious that the maximum gas sensitivity is expected for grain sizes, up to total film thickness, of compact metal oxides around the Debye-length.

In the next section different methods to control gas sensitivity and gas selectivity of a metal oxide are discussed. The main part is focusing on controlling the gas sensitivity by the field effect. The most interesting model for this method is the Wolkenstein model. This model, which was presented in the early sixties, investigates the relationship between the catalytic surface and electronic bulk properties and can explain many experimental data today, which can be seen as a proof to the fact that the chemisorption mainly occurs at the surface of a compact thin-film, having a highly dense structure.

### 3. Gas sensing properties of an Insulated-gate thin-film tin dioxide transistor

#### 3.2 Control selectivity and sensitivity

A desirable property of a gas sensor would be to adjust the sensitivity for different gases. Such a property arises the possibility to individually measure the concentration of gases in a mixture of many gases. The key to control this, according to Wolkenstein's model, is the Fermi level. According to the availability of conduction electrons, that is the local position of the Fermi level, a distribution of differently charged oxygen vacancies will be accomplished. As mentioned earlier, the balance of conduction electrons and charged oxygen vacancies of the bulk must fulfil charge neutrality, or alternatively, Poisson's equation in the case of coverage of oxygen ions at the surface. By interactions of gas molecules or an applied bias voltage, for an Insulated-gate FET, relatively complicated doping profiles arises. Heuristically, the amount of conduction electrons and charged oxygen vacancies decreases and increases, respectively, by forcing the Fermi energy of an n-type metal oxide deeper into the band gap. The adsorption probability for oxidising gases like  $\text{NO}_2$  ( $\text{CO}_{\text{AIR}} + \text{O}^-_{\text{SURFACE}} \rightarrow \text{CO}_{2\text{AIR}} + e^-_{\text{BULK}}$ ) is increased. The amount of conduction electrons and charged oxygen vacancies increases and decreases, respectively, by forcing the Fermi energy of an n-type metal oxide closer to the conduction band. The adsorption probability for reducing gases like  $\text{CO}$  ( $\text{CO}_{\text{AIR}} + \text{O}^-_{\text{SURFACE}} \rightarrow \text{CO}_{2\text{AIR}} + e^-_{\text{BULK}}$ ) is increased.

##### 3.2.1 Methods

There are different methods available to measure concentration of individual gases in a mixture of many gases, or in other words, to control selectivity and sensitivity of a metal oxide. Here methods concerning displacement of the Fermi energy level are discussed. For metal oxide semiconductors, these are:

- Temperature
- Doping level (oxygen vacancies/material doping)
- Field effect

Temperature variation is conceivable to use for so-called low power sensors. A low power semiconductor gas sensor has its gas sensitive material located on top of a membrane. This can be achieved by wet etching. With this structure it is possible to control the temperature of the gas sensitive material from room temperature to 700°C within 10-100 milliseconds because of the low thermal mass of the membrane.

### 3. Gas sensing properties of an Insulated-gate thin-film tin dioxide transistor

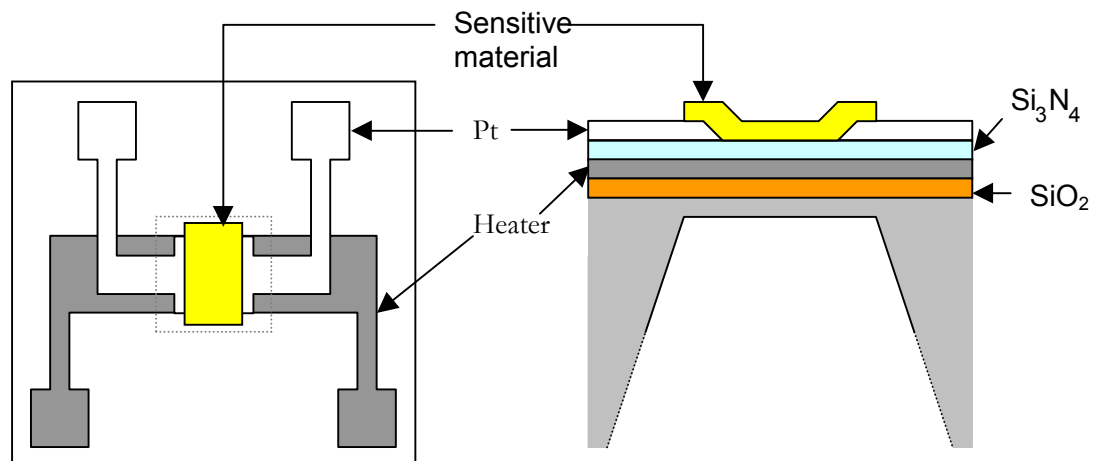


Figure 3.5. Top view and cross section of a low power semiconductor gas sensor. In this example platinum (Pt) is used for sensor contacts. Silicon nitride ( $\text{Si}_3\text{N}_4$ ) is being used as insulator and poly-Si as heater. The dotted rectangle in the middle of the figure on the left is enlarged and showed on the right as a cross section. The gas sensitive material is laying on a so-called membrane. The thermal mass of the membrane is very small.

Another method to affect the Fermi level is to increase the concentration of oxygen vacancies in the crystal structure. If annealing is performed at higher concentrations of nitrogen ( $\text{N}_2$ ) higher conceivable electron densities in the material are possible. However, the doping level of the metal oxide will, if used in atmosphere having normal oxygen level, slowly drift to its equilibrium level. Material doping, e.g. antimony (Sb), indium(In), is also a conceivable method.

#### 3.2.2 Control by external electric field

A gas sensor with a MESFET structure (Metal-Semiconductor FET) might be the easiest conceivable solution to control the Fermi level by field effect, at least theoretically. In reality, problems of the accomplished Schottky-diode from metal to semiconductor can arise, because of the polycrystalline nature of metal oxides. To avoid these a MOSFET gas sensor has been developed and tested by Micronas and Fraunhofer IPM. The backend process and characterisation of this sensor is an experimental part of this final thesis. As for standard MOSFETs, the Fermi level of this sensor is affected by a bias voltage. The concept is to construct a gas sensor with system-on-chip solution. This is achieved by operating the sensor at a relatively low temperature. The idea and the expectation is that an electric field can compensate this.

### 3. Gas sensing properties of an Insulated-gate thin-film tin dioxide transistor

At Fraunhofer IPM in Freiburg, gas measurements of  $\text{NO}_2$  and CO have been performed earlier, using a MOSFET. Figure 3.6 illustrates the layout of this transistor.

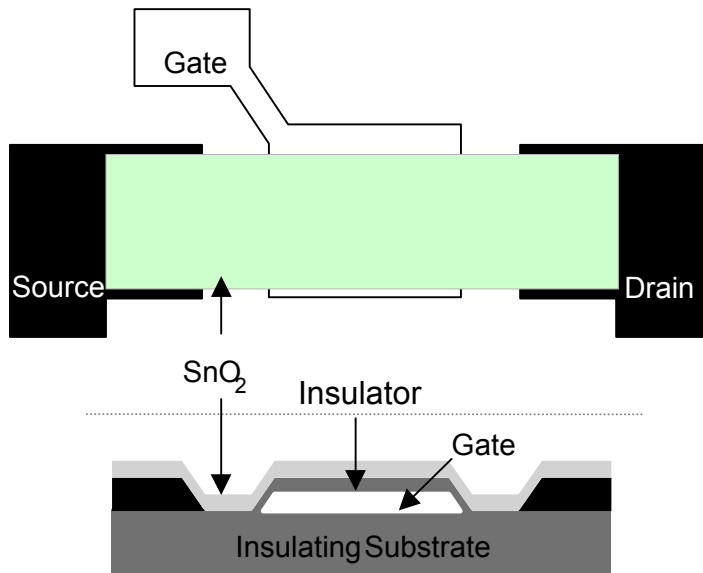


Figure 3.6. Top view and cross section of a tin dioxide ( $\text{SnO}_2$ ) MOSFET.

This transistor clearly illustrates the concept with a MOSFET gas sensor. The Fermi level affects the adsorption probability of gases. The Fermi level of the tin dioxide layer increases when a positive gate voltage is applied and decreases when a negative gate voltage is applied. The high field strength influences the entire tin dioxide layer, while its thickness is in magnitude of the Debye-length ( $\sim 60$  nm). Performed measurements of the gas sensor, illustrated in figure 3.6, showed that the tin dioxide had a slow drift in conductivity when applying a constant gate voltage and by exposure to a static gas composition. This drift stabilised to a new equilibrium point after some hours. A possible explanation of this phenomenon would be a change of oxygen vacancy concentration across the bulk (J.Wöllenstein, M.Jägle, H.Böttner – *A gas sensitive tin dioxide thin-film transistor*). An applied negative gate voltage causes a slow increase of charged oxygen vacancies near the tin dioxide surface, resulting in higher conductivity in this region. An applied positive gate voltage causes a drift of charged oxygen vacancies deeper into the bulk and, consequently, decreases the conductivity near the surface. The drift of oxygen vacancies also affects the adsorption and desorption of gases at the thin-film surface. Gate voltage pulsed operation (GVPO), a non equilibrium method, can be used to avoid this problem. The slow drift can be neglected when the gate voltage varies in different steps and the measurements are done at the end of each interval having a constant gate voltage potential (figure 3.7).

### 3. Gas sensing properties of an Insulated-gate thin-film tin dioxide transistor

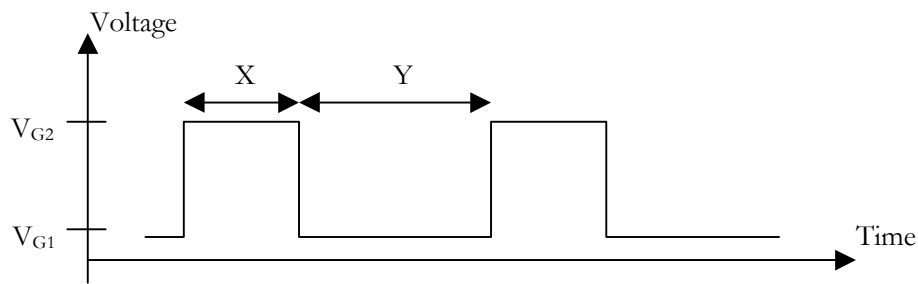


Figure 3.7. Illustration of gate voltage pulsed operation. The gate voltage periodically shifts between two different voltage potentials. The time intervals "x" and "y" are from less than 1 second up to a few seconds. These intervals are needed because it takes a short time to reach the equilibrium point, the drift disregarded. Stable data can be read at the end of each interval having constant gate voltage potential.

A positive gate voltage increases the adsorption probability to reducing gases (e.g. carbon monoxide) and a negative gate voltage increases the adsorption probability to oxidising gases (e.g. nitrogen dioxide). The concentration of, for example, carbon monoxide and nitrogen dioxide is therefore favourable to measure at the end of the positive and the negative pulse, respectively. A spectral analyse of the sensor signal during gate voltage pulse operation could, by identifying different frequency components to different gases, increase the selectivity.

#### 3.2.3 Wolkenstein model

This model is being studied here since it consistently describes electronic and catalytic behaviour of Metal-Oxide semiconductor surfaces from a quantum-chemical point of view. Here, only the interactions between acceptor-like species of the gas phase (oxidising gases, e.g. oxygen) and the chemisorption sites are considered.

Two parameters that influence the adsorption of oxygen discussed earlier are temperature and concentration of adatoms (in this case  $N(O_2)$ ). These parameters are relevant to study chemisorption. Wolkenstein isotherm (H.Geistlinger, 1993)

$$\theta(p) = \frac{\beta p}{\beta p + 1}$$

$$\beta = b \left\{ f^0 \left[ 1 + \frac{v^-}{2v^0} \exp\left(\frac{E_F - E_C}{kT}\right) \right] \right\}^{-1}$$

### 3. Gas sensing properties of an Insulated-gate thin-film tin dioxide transistor

gives a ratio,  $\theta$ , of the total number of chemisorbed species and the number of chemisorption sites of the semiconductor. External parameters like the gas pressure,  $p$ , and the temperature,  $T$ , are involved, but also parameters, which describe the electronic state of the semiconductor,  $E_f$  (Fermi level),  $E_c$  (conduction level) etc. The total coverage ratio,  $\theta$ , can be separated into the coverage of neutral weak-chemisorbed states,  $\theta^0$ , and the coverage of charged strong-chemisorbed states,  $\theta^-$ .

$$\theta = \theta f^0 + \theta f^- = \theta^0 + \theta^-$$

where  $f^0$  and  $f^-$  are probabilities. These two discrete states are central in Wolkenstein's model.

#### Neutral weak-chemisorbed state:

A single adelectron promotes a weak binding of the adatom to the surface atom. These bindings induce electron traps. The weak-chemisorbed state is the precursor state of the strong-chemisorbed state.

#### Charged strong-chemisorbed state:

Single-pairing of a conduction band electron and the adelectron leads to a strong binding and a charge transfer from the semiconductor to the adatom occurs, for acceptor-like chemisorption. The probability that a free conduction band electron is captured by the weak-chemisorbed state, and that a charge transfer from the semiconductor bulk to the adsorption site occurs, is given by the Fermi-Dirac probability.

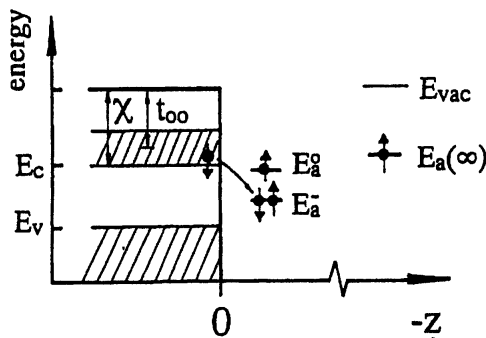


Figure 3.8. Energy diagram for chemisorbed adatoms in an n-type semiconductor; the neutral weak-chemisorbed state  $E_a^0$  and the charged strong-chemisorbed state  $E_a^-$ .  $E_a(\infty)$  denotes the energy level for the gas particle at infinite distance from the surface,  $T_{oo}$  the centre of the conduction band,  $E_{vac}$  vacuum energy level and  $\chi$  work function. A free conduction band electron (so-called "free valence" of the surface) can be trapped by the weak-chemisorbed adatom (H.Geistlinger, 1993).

### 3. Gas sensing properties of an Insulated-gate thin-film tin dioxide transistor

The probabilities  $f^o$  and  $f^-$  ( $f^o + f^- = 1$ ) depend on the Fermi level and energies of conceivable quantum states, two states for weak-chemisorption (two electron spin directions) and one for strong-chemisorption. The remaining parameters of Wolkenstein's isotherm denotes photon frequencies,  $\nu^-$  and  $\nu^o$ , and a factor that relates the amount of adatoms that reach the surface of a metal oxide,  $b$  (dependent on gas pressure, temperature etc.).

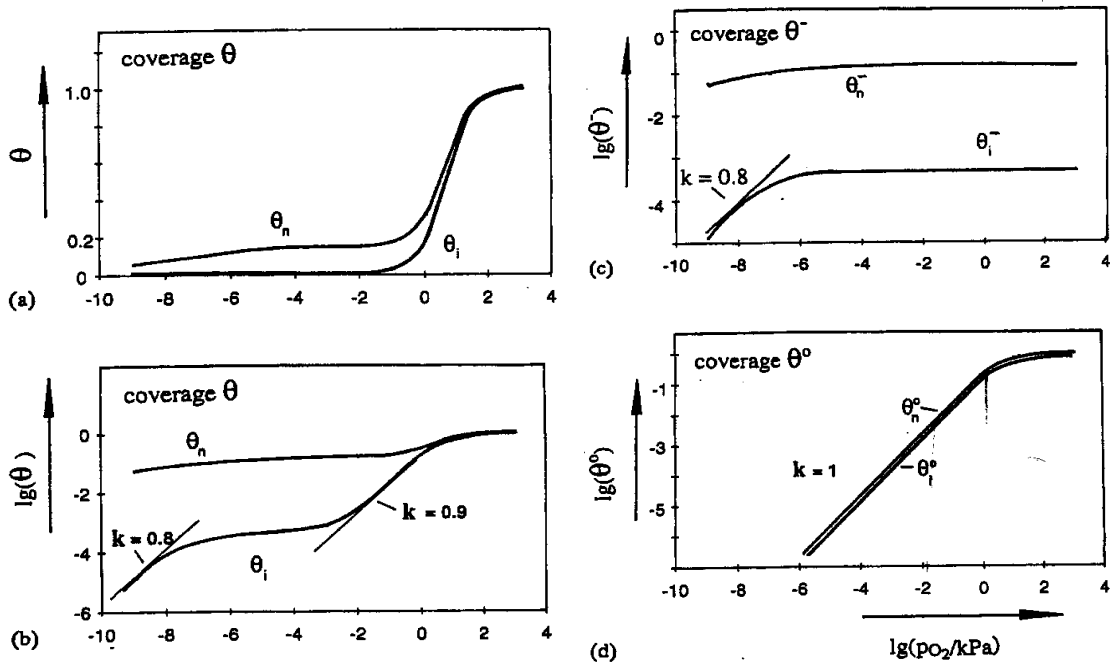


Figure 3.9. Chemisorption of  $O_2^-$  on thin ZnO film according to Wolkenstein isotherm ( $E_g=3.2$  eV,  $E_{d1}=-0.05$  eV,  $E_{d2}=-0.4$  eV,  $E_{A^-}(O_2^-) - E_{A^o}(O_2^-) = -1.1$  eV,  $E_{A(\infty)}(O_2^-) - E_{A^o}(O_2^-) = 0.1$  eV). The graphs are calculated for  $T=480\text{K}$  and for two different oxygen-vacancy concentrations:  $[V_o]=10^{12}$   $\text{cm}^{-3}$  (index  $i$ ) and  $[V_o]=10^{17}$   $\text{cm}^{-3}$  (index  $n$ ). Example is from paper *Electron theory of thin-film gas sensors* (Geistlinger, 1993).

An example of Wolkenstein isotherm is shown in figure 3.9. The term  $\beta$  of Wolkenstein isotherm for doping concentration  $i$  is near constant in the low-pressure region,  $10^{-10} - 1$  kPa. The reason is that the probability factor for weak-chemisorbed adatoms is very small ( $f^o \ll 1$ ) in this region. This results in a linear relationship between chemisorbed coverage  $\theta_i$  and gas pressure  $p$ . The deviation, clearly seen in the logarithmically represented diagram for the total coverage  $\theta$ , is caused by the pressure dependence of  $\beta$ .

$$\theta_i (10^{-10} < p_{O_2} < 1\text{kPa}) \propto \beta p$$

### 3. Gas sensing properties of an Insulated-gate thin-film tin dioxide transistor

For doping concentration  $n$  the chemisorbed coverage  $\theta_n$  is independent from pressure in the same region.

$$\theta_n (10^{-10} < p_{O_2} < 1 \text{ kPa}) \sim \text{constant}$$

For pressures below  $10^{-4}$  kPa is  $f^- \sim 1$ , which means that the strong-chemisorbed coverage dominates over the weak-chemisorbed coverage in the low-pressure region. Further, already at  $\sim 10^{-6}$  kPa are  $\theta_i^-$  and  $\theta_n^-$  both saturated. Above  $10^{-3}$  kPa and 1 kPa (not shown) is  $\theta_i^o$  and  $\theta_n^o$ , respectively, larger than  $\theta_i^-$  and  $\theta_n^-$ . This is the reason why only a fraction of the adsorbed gas molecules can switch over to a chemisorbed site.

### 3. Gas sensing properties of an Insulated-gate thin-film tin dioxide transistor

#### **3.3 Control of the Fermi energy level of an Insulated-gate thin-film tin dioxide transistor having a multigate structure**

This section deals with how the adsorption probability of gases for an Insulated-gate field effect thin-film tin dioxide transistor could be modulated by different bias voltage potentials along the channel.

The sensitivity to gases can be defined as:

$$S = \frac{R}{R_0}$$

$R$  : resistance by gas exposure.

$R_0$  : base line (normal oxygen concentration at atmospheric pressure).

The following heuristical picture motivates a multigate structure.

The sensitivity for the reducing gas CO is high for the gate-channel potential,  $V_{\text{channel}} = +3 \text{ V}$  for a certain sensor. Further, to achieve a good base line of this sensor the drain-source voltage is chosen to,  $V_{\text{DS}} = +5 \text{ V}$ . The gate voltage could, consequently, be set to  $+8\text{V}$ , for instance. This would give a correct gate-channel potential near the drain, but would result in a gate-channel potential far from a favourable one near the source. The sensitivity will be higher near the drain than near the source. This situation is illustrated in figure 3.10a. Supposing, the gate-channel voltage near the source could be modulated by a separate gate electrode situation b, in the figure, is valid.

### 3. Gas sensing properties of an Insulated-gate thin-film tin dioxide transistor

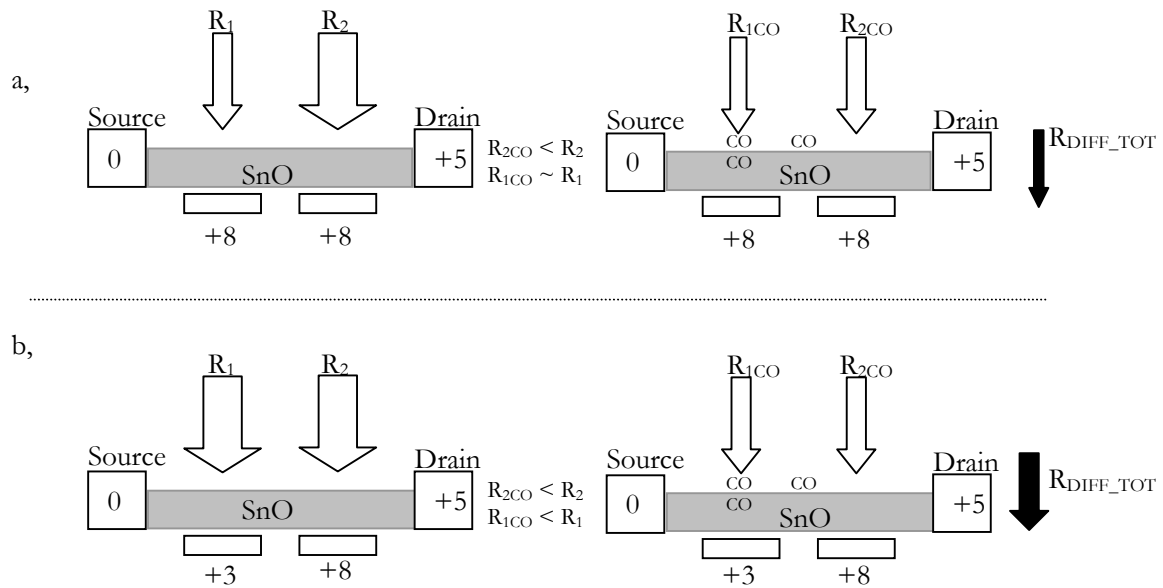


Figure 3.10. Illustration of control of Fermi energy gradient. a, MOSFET gas sensor structure with 2 gates at equal potentials without (on the left) and with (on the right) interactions with carbon monoxide. b, MOSFET gas sensor structure with 2 gates at different potentials without (on the left) and with (on the right) interactions with carbon monoxide. The total resistance drop by exposure to carbon monoxide is expected to increase for the second scenario. The width of the arrows corresponds to resistance levels.

The sensitivity for this example is defined as

$$S = \frac{R_{1CO} + R_{2CO}}{R_1 + R_2}$$

The aim with the multigate structure is to achieve a specific operation point,  $V_{ds}$  and  $I_d$ , where the gate-channel voltage is kept at a constant level along the channel and where the gas sensitivity and the gas selectivity is good. To study the problem of how the electric field is spread more thoroughly one must investigate the superposition of the fields shaped by each individual bias voltage.

The remaining part of the report discusses the experimental part. First, the backend process of the sensor is presented. Afterwards, the construction of an electronic system to perform gate voltage pulsed operation and solutions to control chip temperature are described. Finally, gas measurements of the sensor are evaluated.

### 4. Technology – experimental

The first section of this chapter deals with modern transistor technologies and available technologies for FET-based semiconductor gas sensors. The second section describes the layout of the developed sensor. The third and fourth section is about the technology used by Micronas and the technology used in this work to manufacture the sensor, respectively.

#### 4.1 Transistor technologies

##### 4.1.1 Definitions

Mainly, there exist two different types of transistor technologies, CMOS; which offers small area, high input resistance, low power consumption, bi-directional current switching, inherent memory capability etc. and the bipolar transistor; which offers high current drive per unit area, good matching, superior linear performance, low sensitivity to process variation etc. (Elmasry M.I, 1994). In the late 90ths BiCMOS, a combination of CMOS and bipolar transistors, became a common technology.

There are two main different types of FETs; Insulated-gate field effect transistors (IGFET) and Junction field effect transistors (JFET). A MOSFET is the most representative transistor among IGFETs within modern electronics. CMOS, which stands for complementary Metal-Oxide-Semiconductor field effect transistor, is a very common technology. The technology is a mixture of p-type and n-type MOSFETs.

##### 4.1.2 FET-based semiconductor gas sensors

Two FET-configurations are conceivable to control the adsorption probability of gases by an electric field that can be modulated (J.Wöllenstein, M.Jäggle, H.Böttner – *A gas sensitive tin dioxide thin-film transistor*); an Insulated-gate field effect transistor (IGFET) and a Metal-Semiconductor field effect transistor (MESFET). The sensor is arranged as a thin-film transistor. The gate, for an IGFET, is buried below an insulator. For a MESFET thin-film gas sensor the drain current is modulated by the accomplished Schottky-diode across a gate contact and a gas sensitive substrate.

The gas sensor analysed in this final thesis is an IGFET. Principally, the manufacturing processes for gates and insulator have been developed by Micronas and the processes for source/drain contacts and gas sensitive material are an experimental part of the final thesis. In the following sections these processes are going to be described more thoroughly.

### 4.2 Sensor layout

Sensors are manufactured using six inches wafers and consist of sensor layouts developed in co-operation with Micronas and Technical University of Illmenau, Professorate Solid State Electronics. Only two different layouts are shown in this section (figure 4.1).

The size of a chip is 3\*3 mm. Along the sides of the chip there are bond pads for source, drain, gates, platinum heater electrode, platinum temperature sensor and a diode temperature sensor. Additionally, there is a poly-silicon heater electrode, with corresponding pads, for some layouts. The sensor element/elements, consisting of a thin-film of metal oxide, is/are located near the heater electrode.

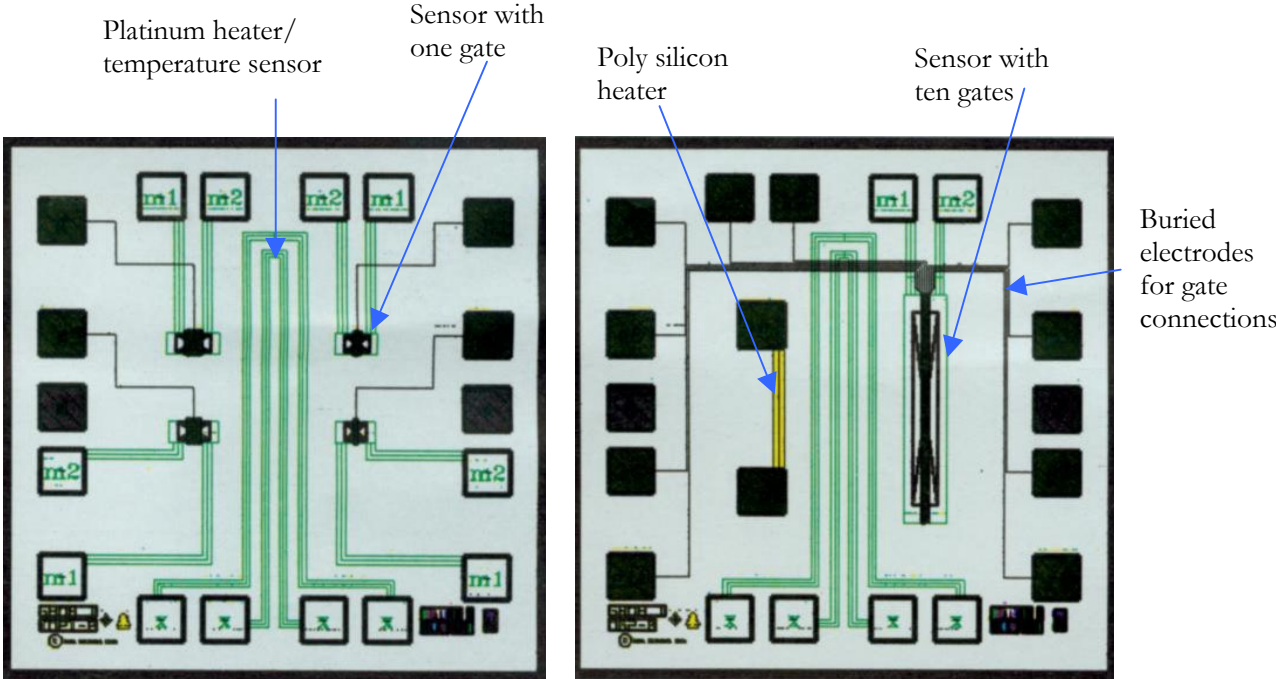


Figure 4.1. On the left: Sensor with one gate. On the right: Sensor with ten gates.

### 4.3 Technology – Buried gates

The realisation of the sensors consists of several process steps. Most of these were developed and fabricated by Micronas.

All sensor layouts have one or more metal electrodes. The idea is that the conductivity of the gas sensitive material will change when different voltage potentials are applied at these electrodes. Because of the resemblance to the gate of a FET these electrodes can be seen as transistor gates.

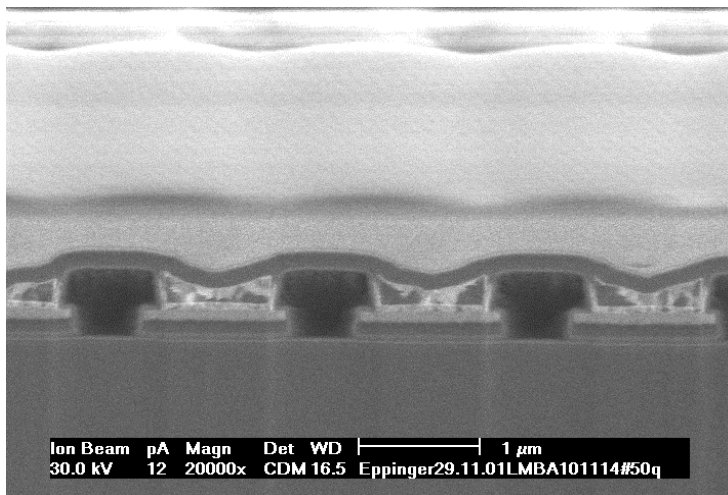


Figure 4.2. Scanning electron microscope (SEM) picture of gate electrodes.

### 4.4 Experimental – platinum electrodes and gas sensitive material

Deposition of platinum layers and gas sensitive materials are an essential part of the final thesis.

#### 4.4.1 Deposition of platinum

Platinum is commonly used for gas sensors as electrode material and for resistive heater/temperature sensor element. The most important reason is that it does not oxidise at temperature of interest for this application. The other advantage of using platinum is the close to linear relationship between resistance and temperature.

In this work platinum electrodes are used to heat the sensor to operation temperature, as temperature sensing element, for connections to the metal oxide (source and drain) and for the top layer of the gate pads. Platinum for source, drain (including their pads) and heater/temperature sensor is deposited onto the insulator layer.

The used process for platinum includes the structuring with help of a aluminium sacrificial layer. The sacrificial layer is used to improve the lift-off behaviour and to get a smooth edge of the electrodes for improving the overgrowth of the sensitive material.

The technologies used to deposit platinum are:

- aluminium deposition – 280 nm
- photolithographic process
- aluminium wet etching
- tantalum deposition – 25 nm
- platinum deposition – 200 nm
- lift-off process
- aluminium wet etching

The first step is to deposit 280 nm aluminium onto the substrate by evaporation. Vacuum evaporation was performed by electron-bombardment on a Al-source. The heat causes molecules to evaporate and leave the solid surface. The kinetic energy needed for a molecule to evaporate, which is pressure dependent, corresponds to the attracting intermolecular forces in the material. The gas particles are transported from the evaporation target to the wafer, where they are deposited. The deposition rate was measured using quartz plates. Electrodes on opposite sides of the quartz plates

#### 4. Technology - experimental

---

connected to an oscillating cause vibrations. The resonance frequency of the vibration will change when the deposited film thickness increases. The deposition rate is controlled automatically.

The aluminium is followed by a photolithographic process. A photolithographic process allows a stencil structure to be printed in photoresist. The photoresist is spun onto the substrate. The stencil structure is achieved after exposure from UV light through a mask and development using an aqueous solution.

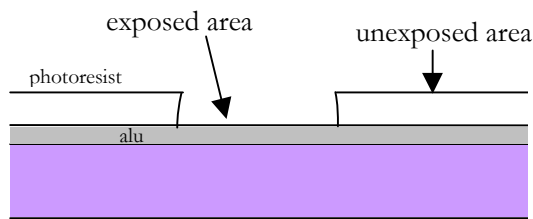


Figure 4.3. Current state of the process.

The aluminium is a sacrificial layer. It must be removed before the tantalum/platinum is deposited onto the wafer. This is achieved by wet etching. Etch processes fall into two broad categories; isotropic and anisotropic etch processes. While isotropic etchants attack the material being etched at the same rate in all directions, anisotropic etchants attack at different rates in different directions. For the aluminium an isotropic wet etching process is used and it results in a so-called undercutting effect, which means that aluminium horizontally under the photoresist etch mask is gradually being etched during the etch procedure. This phenomena is the purpose of the sacrificial layer.

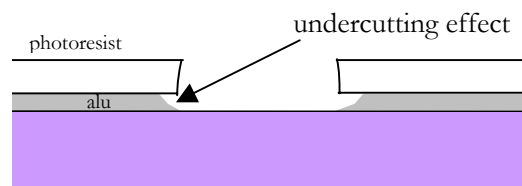


Figure 4.4. Illustration of aluminium wet etching.

#### 4. Technology - experimental

---

The remaining process steps for the platinum deposition are illustrated in figure 4.5.

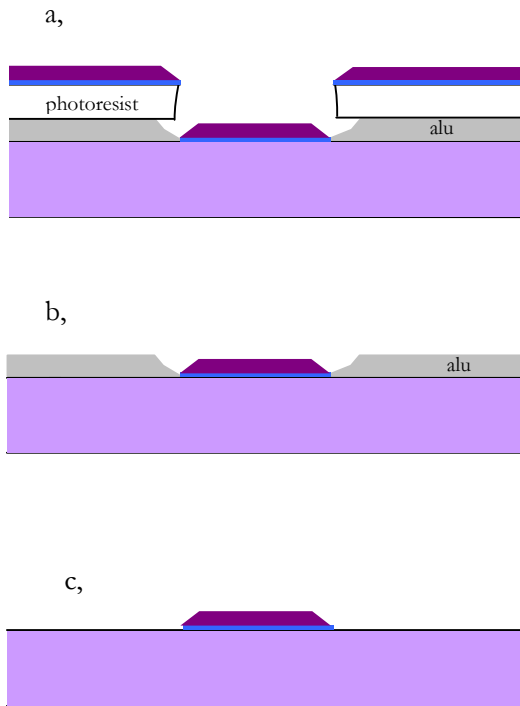


Figure 4.5. a, Deposition of 25 nm tantalum and 200 nm platinum by evaporation. b, Lift-off process; the photoresist is dissolved and the overlying tantalum/platinum is "lifted off". c, Aluminium wet etching.

In contrast to Micronas standard processes, in this thesis deposition followed by a lift-off process is used. Micronas only uses etch techniques to structure their chips. The drawback with lift-off processes is that not all materials on top of the photoresist might be lifted. A big advantage, though, is that an individual etch procedure does not have to be developed. Further, not all material, like platinum, are conceivable to structure using an etch technique. Therefore, lift-off processes are beneficial for research work.

A smooth junction between the platinum and the surrounding material is established. This structure was accomplished by the sacrificial aluminium layer and is needed to achieve a good contact between the platinum and the metal oxide, whose deposition technique will be described next.

## 4. Technology - experimental

---

### 4.4.2 Deposition of gas sensitive material

The technologies used to deposit tin dioxide ( $\text{SnO}_2$ )/tungsten trioxide ( $\text{WO}_3$ ) are:

- photolithographic process
- tin dioxide/tungsten trioxide deposition
- lift-off process

The deposition technique used for the metal oxide is sputtering. A process where atoms of a solid surface are removed due to energetic particle bombardment is called sputtering. It occurs either when a hot plasma and solid interact with each other or when energetic particles hit a surface. The first phenomena can be observed at the moon surface due to the impact of solar wind. An example of the second phenomenon is radiation of energetic particles by radioactive decay. Within the semiconductor industry sputtering is used for etching and thin-film deposition. The wafer is the solid target that is being sputtered for an etch procedure and the substrate for the sputtering process for thin-film deposition.

#### 4.4.2.1 Tin dioxide

The crystal structure of tin dioxide is shown in figure 4.6. Every tin atom (small globe) is surrounded by six oxygen atoms (big globe), in turn connected to three tin atoms in the crystal structure (Wöllenstein, 1997). This crystal structure is an insulator. Semiconducting properties arise first when oxygen vacancies exist. For cassiterite, the mineral where tin dioxide is found in the nature, oxygen vacancies always exist because the material is never entirely oxidised.

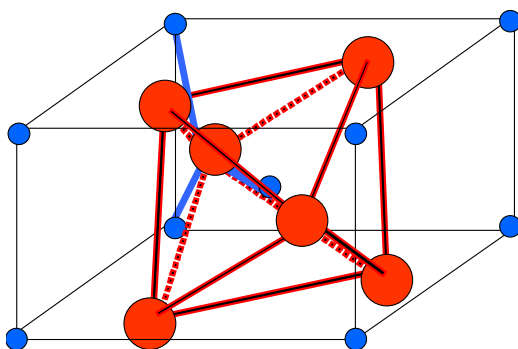


Figure 4.6. Illustration of the tetragonal crystal structure of tin dioxide.

## 4. Technology - experimental

---

The substrate is sputtered twice for the deposition procedure used, each time 3 minutes, with a radio-frequency (RF) power of 1.5 kW in an argon plasma (cleaning process of the surface). The target, SnO<sub>2</sub>, is sputtered twice in a argon-oxygen plasma using a radio-frequency (RF) power of 0.5 kW, each time 6.6 minutes.

### 4.4.2.2 Tungsten trioxide

Another gas sensitive material that has been tested is tungsten trioxide, WO<sub>3</sub>. As tin dioxide, tungsten trioxide is a polycrystalline material and is an n-channel conductor when oxygen vacancies exist. Its crystal structure varies with the temperature. Each phase is, however, a modification of a so-called octahedral structure (Pohlmann, 2001) shown in figure 4.7.

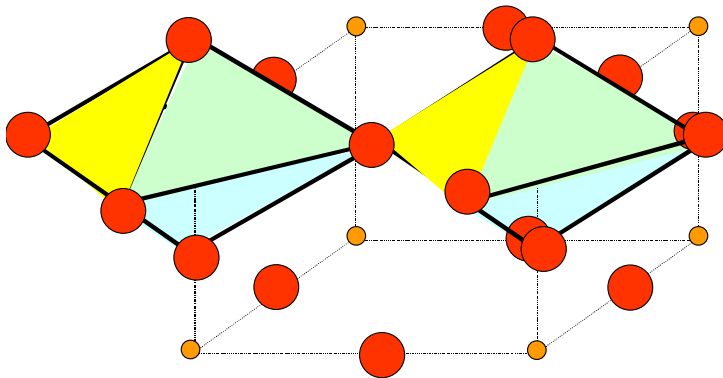


Figure 4.7. WO<sub>3</sub> – structure. Two WO<sub>6</sub> – octahedra are illustrated at two of the corners of the square in thin lines.

Tungsten trioxide is deposited by so-called reactive sputtering from a tungsten target in an argon-oxygen plasma. The radio-frequency (RF) power was 0.25 kW and the sputtering process lasted 94 minutes. The sputtered tungsten oxidises first on the wafer.

The most important difference between these two metal oxides is that tungsten trioxide has lower conductivity than tin dioxide. The distance needed to screen the electric field, the Debye-length, is therefore longer for tungsten trioxide than for tin dioxide. Further, the Debye-length also varies with temperature and the concentration of charge carriers. Together, these two materials give the opportunity to investigate how well the conductivity of the metal oxide can be controlled for this transistor technology, in particular by exposure to different gas concentrations at different operation temperatures.

## 4. Technology - experimental

### 4.4.3 Results of backend process

The experimental part resulted in these sensors.

Table : Developed sensors with corresponding annealing time, metal oxide thickness and deposition technology. The thickness of the insulator, silicon nitride, varied from 150 nm up to 250 nm.

SENSOR	Annealing time at 400°C	Thickness (metal oxide)	Deposition technology (metal oxide)
WO <sub>3</sub> – 150 nm Si <sub>3</sub> N <sub>4</sub>	70 h	125 nm	Sputtering
WO <sub>3</sub> – 200 nm Si <sub>3</sub> N <sub>4</sub>	21.5 h	125 nm	Sputtering
WO <sub>3</sub> – 250 nm Si <sub>3</sub> N <sub>4</sub>	-	125 nm	Sputtering
SnO <sub>2</sub> – 150 nm Si <sub>3</sub> N <sub>4</sub>	111 h	75 nm	Sputtering
SnO <sub>2</sub> – 200 nm Si <sub>3</sub> N <sub>4</sub>	111 h	75 nm	Sputtering
SnO <sub>2</sub> – 250 nm Si <sub>3</sub> N <sub>4</sub>	70 h	55 nm	Evaporation

The sputtered tungsten trioxide, 125 nm, was too high-resistive. Further, the sputtered tin dioxide, 75 nm, was very low-resistive (chapter 6. *Measurement and conclusions*). Therefore, mainly, the characteristics of sensors with tin dioxide deposited by evaporation, 55 nm, were analysed. Chips were mounted at TO5 housings with gold thread.

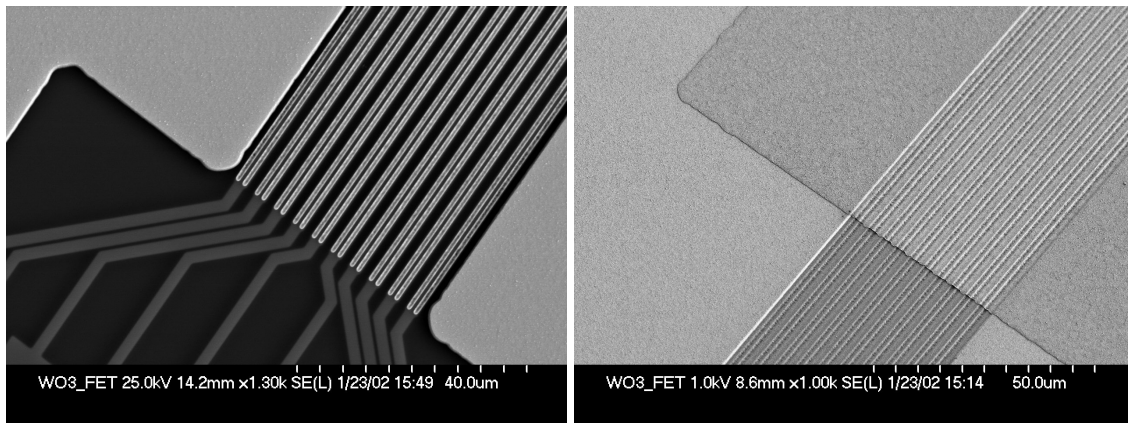


Figure 4.8. On the left: A part of a ten gate electrode structure. Each gate consists of two adjacent metal electrodes for this sensor layout. On the right: A tungsten trioxide layer on top of the source and the drain contact and the gates in the middle.

#### 4. Technology - experimental

---

There were some more or less critical steps for the technologies tested in this experimental part. The heater electrodes and source/drain contacts were partly laying on top of the connection electrodes for the transistor gates, with insulating layers in between. At an early stage it was investigated that no short-circuits existed between these connection electrodes and platinum structures. Analysis of the metal oxide layer at the platinum edges also showed a satisfactory result, thanks to the aluminium sacrificial layer. However, the platinum layer for the gate pads did not succeed entirely. After annealing, the platinum pads were damaged. Also gate pads without an overlying platinum layer were damaged by the annealing process. This problem was, however, not consistent. Most parts of the wafer with evaporated  $\text{SnO}_2$  (250 nm  $\text{Si}_3\text{N}_4$ ) seemed to be unaffected by the annealing process, at least after 70 hours annealing.

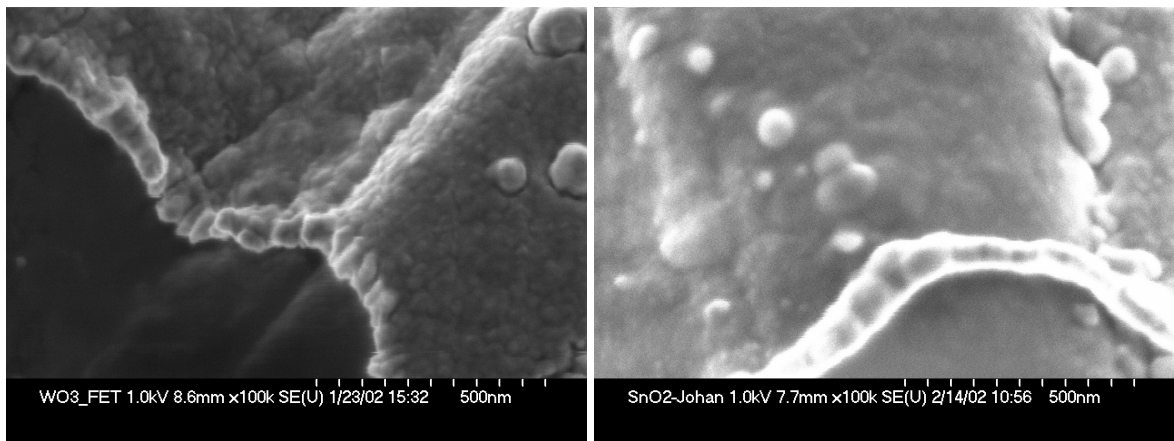


Figure 4.9. On the left: A tungsten trioxide layer. The grains of the material are around 20-50 nm and are following the curved contour of the insulator/gate-interface. On the right: A tin dioxide layer. One can observe a visual gap between the tin dioxide and the gate/dielectric layer-structure below. This effect is caused by the insulator, silicon nitride, in between. Both these metal oxide layers ( $\text{WO}_3$  on the left and  $\text{SnO}_2$  on the right) are deposited by sputtering.

## 5. Experimental – gate voltage pulsed operation and temperature control

### 5. Experimental – gate voltage pulsed operation / temperature control

This chapter is about the design and the implementation of gate voltage pulsed operation. In addition, a design of a controller for sensor operation temperature via the on-chip platinum heater is investigated.

#### 5.1 Control of gate voltages

The constructed electronics consist of two printed circuit boards; one for power supply realisation and one for realisation of the logic to accomplish the specification (section 5.1.1 *Specification*). The layout is made in Mentor Graphics - Integra, a software for Printed Circuit Board (PCB) design. The construction is encapsulated in an aluminium chassis.



Figure 5.1. Construction of gate voltage pulsed operation. The front panel has switches to select pulse mode, temperature pulsed or gate voltage pulsed operation, and to select the sign (positive or negative potential) for the gate voltage pulsed operation mode. Temperature pulsed operation is a method to heat a sensor with controlled heat intervals. Further, the front panel has an output for trigger functions.

## 5. Experimental – gate voltage pulsed operation and temperature control

### 5.1.1 Specification

The hardware to control the sensor's gate potentials is based on the gate voltage pulsed operation (GVPO) concept. The period time, the duty cycle and the output voltage levels are adjustable. It is also possible to have constant output voltages.

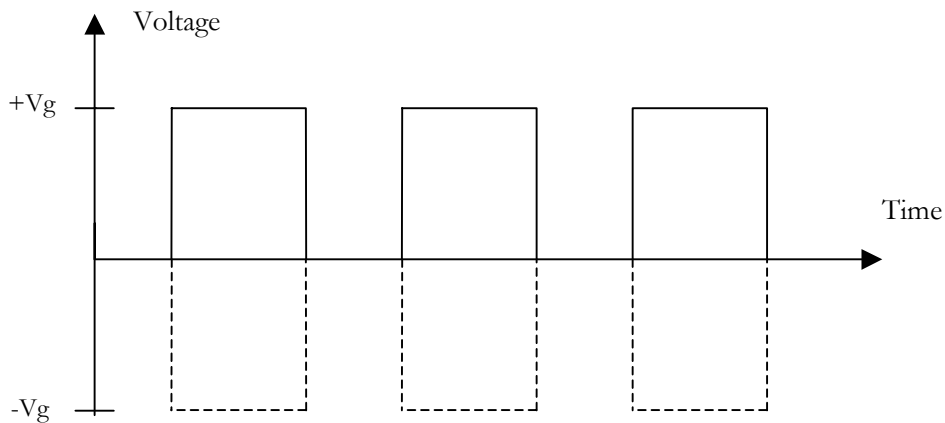


Figure 5.2. Gate voltage pulsed operation; solid line and dashed line shows a pulse with positive and negative potential shifts, respectively.

Ten different pulsed voltage levels are available as outputs. The purpose is to be able to measure with different voltage potentials applied to the different gates of the gas sensor.

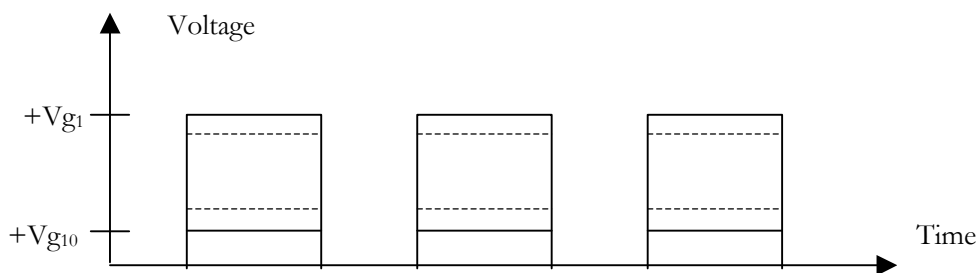


Figure 5.3. Illustration of output signals. The figure shows an example for positive voltage shifts, where  $V_{g1}, \dots, V_{g10}$  satisfies the relationship:  $V_{g10} \leq V_{g9} \leq \dots \leq V_{g1}$ .

## 5. Experimental – gate voltage pulsed operation and temperature control

The voltage potentials fulfil:

$$0.5 < |V_{g_N}| < 10 \quad , N = 1, 2, \dots, 10$$

$$|V_{g_{10}}| \leq |V_{g_9}| \leq \dots \leq |V_{g_1}|$$

The negative pulse can also be driven from a power operational amplifier. This arises the possibility to use the pulse for temperature pulsed operation. This is a method to heat the sensor with controllable heat intervals (R. E. Cavicchi etc., 1996). The temperature pulsed operation signal has a drive current of 500 mAmps as maximum rating up to 10 V.

There is a trigger pulse available as output. The trigger pulse is defined as low signal level and is generated shortly before each pulse shift. The time range of the trigger pulse is from milliseconds up to 1 second. The output for the trigger signal is TTL compatible. The idea having a trigger pulse is to perform one measurement before each voltage shift with help from a measurement instrument like a digital voltmeter or Semiconductor Parameter Analyser by connecting it to an external trigger input.

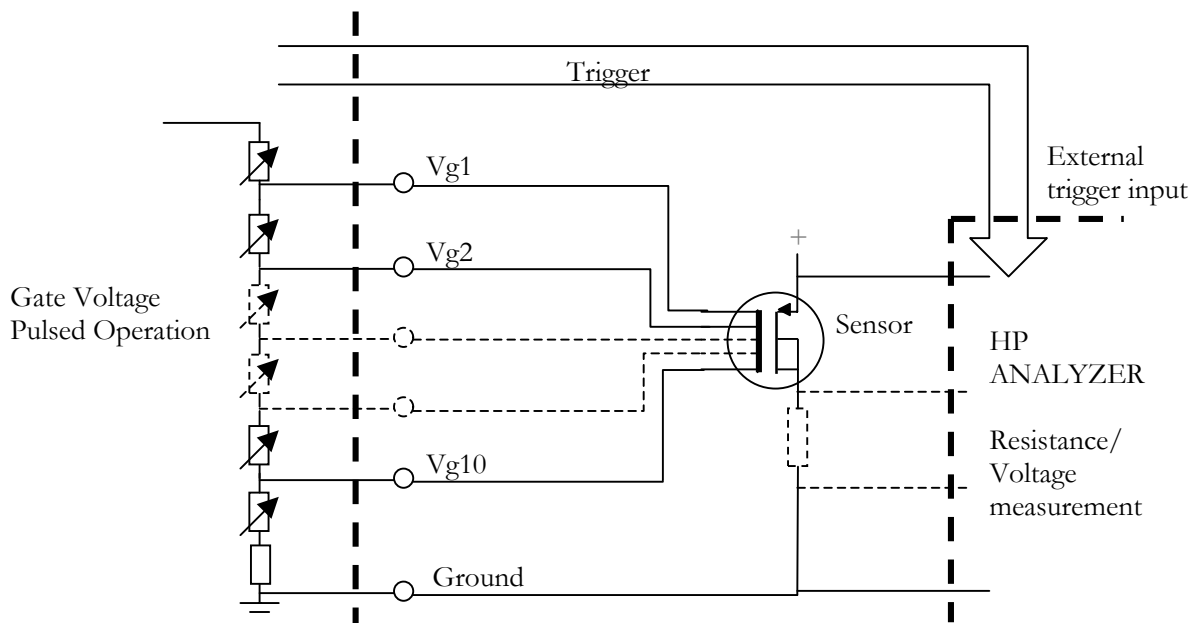


Figure 5.4. Example of measurement set up for a sensor with multigate structure.

## 5. Experimental – gate voltage pulsed operation and temperature control

### 5.1.2 Realisation of pulse

The main device for realisation of gate voltage pulsed operation is a multi vibrator component, NE555 (reference : datasheet 1).

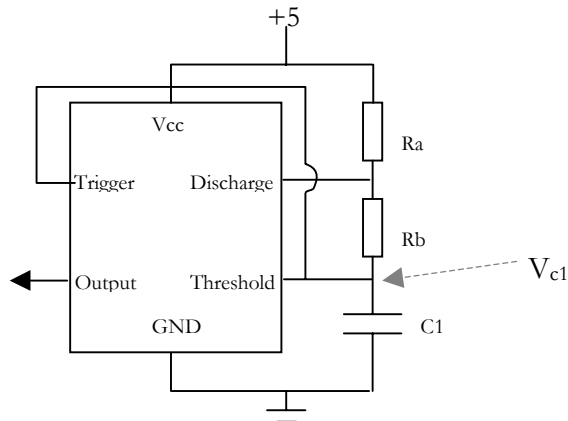


Figure 5.5. Schematic view of NE555 connections.

The component NE555 has a discharge channel that can logically be turned on or off by a transistor connection. When the discharge channel is turned off the output is defined as logically high. The time elapsed before the voltage potential  $V_{c1}$  (figure 5.5) increases from its lowest value ( $1/3$  of  $V_{cc}$ ) to its highest value ( $2/3$  of  $V_{cc}$ ) is:

$$t_{high} \approx C_1(R_A + R_B) * 0.7 \quad (s)$$

When the voltage potential  $V_{c1}$  reaches  $2/3$  of the voltage potential  $V_{cc}$  the discharge channel is turned on and the output is changed to logically low. The time elapsed before the voltage potential  $V_{c1}$  decreases from its highest to its lowest value is given by the time constant for the discharge channel through the resistance  $R_B$ .

$$t_{low} \approx C_1 R_B * 0.7 \quad (s)$$

Since the output time for high level always is larger or equal to low level a switch to an inverter has been implemented. Thereby, a duty cycle less than 50% is accomplished.

## 5. Experimental – gate voltage pulsed operation and temperature control

### 5.1.3 Realisation of output stages

The output stage for gate voltage pulsed operation is implemented using two operational amplifiers; Ultralow Offset Voltage Operational Amplifier OP07 (reference : datasheet 2). One operational amplifier is configured as inverting, for negative pulse shifts, and one as non-inverting, for positive pulse shifts.

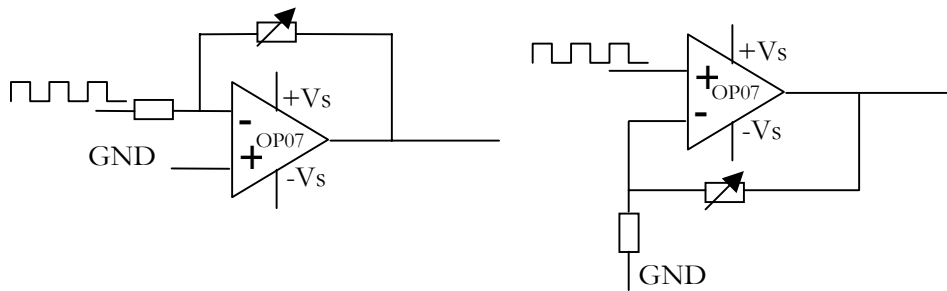


Figure 5.6. Inverting and non-inverting configurations of the output stages for gate voltage pulsed operation.

The temperature pulsed operation mode requires an output stage that can deliver a nominal power up to 1 W. A power operational amplifier is being used for this purpose; 3 Amps Power Operational Amplifier L165V (reference : datasheet 3). The heat pulses are defined as negative.

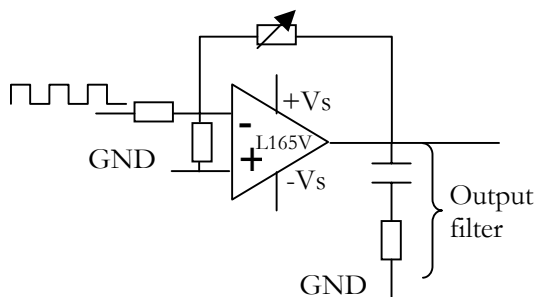


Figure 5.7. Output stage of temperature pulsed operation.

## 5. Experimental – gate voltage pulsed operation and temperature control

### 5.1.4 Realisation of power supply

When constructing an electronic device non-ideal conditions such as noise, temperature variations and nonlinearities of components have to be considered. This is often extra critical for voltage regulation, while one must consider variations in power source, operation variations of heated components and so on. The calculations for the construction of this power supply is not exact, instead estimations of the most critical parts in the construction have been used as design rule.

The realised power supply supports these voltages (DC) with these maximum nominal power levels:

- 12 V - 25 mAmps
- 5 V - 75 mAmps
- -12 V - 500 mAmps

This construction basically consists of three voltage regulators, a transformer and a bridge rectifier.

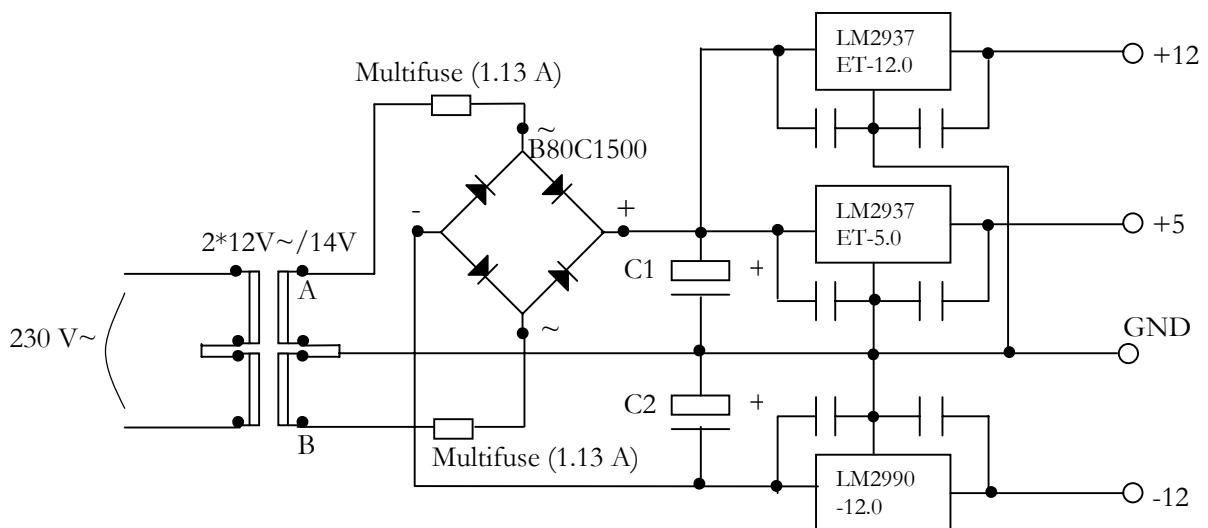


Figure 5.8. Power supply.

The low dropout voltage regulator LM2990 supports at least 1 Amp and has a dropout voltage of typically 0.6 V and regulates the output at -12 V (reference : datasheet 4). To be able to keep -12 V at the output -12.6 V at the input has been used as a guide line for the remaining design. Since the regulated source with -12 V has the highest nominal

## 5. Experimental – gate voltage pulsed operation and temperature control

power, 500mAmps (design specification), this voltage supply decides the size of the transformer and the bridge rectifier. For the remaining calculations this voltage regulator is mainly considered.

The transformer has 2\*12 V~/14 VA at the secondary side. The peak voltage of the alternating current, variations in net voltage and nonlinearities in the transformer disregarded, is:

$$\hat{V}_{OUT} = \sqrt{2} * V_{eff} = \sqrt{2} * 12 \approx 17(V)$$

This is a peak-to-peak value. The voltage at point B in figure 6.8 is inverted in comparison with the voltage at point A. Due to a small voltage drop across the rectifying diodes the peak of the rectified sine wave will be smaller than  $\hat{V}_{OUT}$ . The voltage drop across each diode is around 0.7 V.

For the voltage regulator to be able to keep a constant voltage large capacitors are needed at the bridge rectifier output. At full nominal power, 500 mAmps, the variations of the unregulated voltage is in worst case 10 % of the peak value. The peak and bottom voltage at the output of the bridge rectifier, variations in net voltage disregarded, are therefore estimated according to figure 5.9:

$$\hat{V}_{RECTIFIER\_OUT} = \hat{V}_{OUT} - 0.7 \approx 16.3(V)$$

$$V_{RECTIFIER\_OUT\_min} = \hat{V}_{RECTIFIER\_OUT} - 10\% \approx 14.7(V)$$

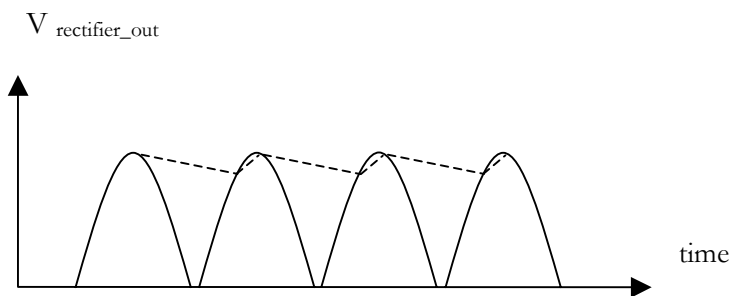


Figure 5.9. Illustration of a full - wave bridge rectified output for positive voltage. Dashed line and solid line shows the voltage with and without output capacitors, respectively.

To analyse the lowest and highest possible unregulated input voltage to the voltage regulator supporting -12 V one must consider variations in net voltage and

## 5. Experimental – gate voltage pulsed operation and temperature control

---

nonlinearities in the transformer with varied current level. The variation in the net voltage is estimated to:

$$V_{NET} = 230 \text{ V} \sim +15\% -10\%$$

The lowest possible unregulated input voltage (absolute value) to the voltage regulator is reached with maximum nominal power and low net voltage, estimated to:

$$V_{REGULATOR\_INPUT\ min} = ((\hat{V}_{OUT} - 10\%) - 0.7) - 10\% \approx 13.1(V)$$

The last decrease with 10% is due to the variation in the unregulated voltage at the input to the voltage regulator at maximum nominal power. With a voltage drop around 0.6 V for the low dropout voltage regulator its output will be able keep -12 V according to these calculations.

In idle operation, that is with no current flowing, the voltage at the secondary side of the transformer rises, because the output voltage 12 V~ is valid at nominal power, 14VA. The highest voltage at the secondary side of the transformer is estimated to:

$$\hat{V}_{TRANSFORMER\_NO\_LOAD} = 1.6 * 12 = 19.2(V)$$

The highest possible unregulated input voltage to the voltage regulator is reached with no load and high net voltage, estimated to:

$$\hat{V}_{REGULATOR\_INPUT} = \hat{V}_{TRANSFORMER\_NO\_LOAD} + 15\% \approx 22.1(V)$$

Maximum allowed operational input voltage for the low dropout voltage regulator LM2937 and LM2990 over its entire operation temperature range is specified to 26 V and -26 V, respectively (reference : datasheet 5, datasheet 4).

The maximum power dissipation for the voltage regulator is expected at high net voltage and at maximum nominal power. The output voltage of the bridge rectifier varies between 16.3 V and 14.7 V according to the calculations above at nominal power.

The maximum power dissipation for the regulator LM2990 is estimated to:

$$\hat{V}_{REGULATOR\_POWER\_DISSIPATION} = ((V_{EFFECTIVE} + 15\%) - 12) * I_{NOMINAL\_POWER} = ((16 + 15\%) - 12) * 0.5 \approx 3.2(W)$$

## 5. Experimental – gate voltage pulsed operation and temperature control

### 5.2 Control of operation temperature

The operation temperature strongly influences adsorption probabilities of gases at the surface of the sensitive material and therefore the gas sensing properties of the sensor. Consequently, it is important to have information about the chip temperature. The MOSFET gas sensor has two platinum electrodes; one intended as heater element and one intended as temperature sensing element. A temperature controller of this SISO (single input single output) system could, for example, consist of a PI-controller or a Lead-Lag filter. However, an alternative principle to regulate the temperature has been analysed where only one of the platinum electrodes is needed. The sensor heater forms a part of a Wheatstone bridge, the power through it is controlled to maintain the heater at a constant resistance. The regulator consists of lead compensate circuit, implemented as a voltage feedback controlled operational amplifier, and a p-channel MOSFET. This construction is based on a controller commercially used for gas sensors produced by Capteur Sensors Ltd (URL – homepage).

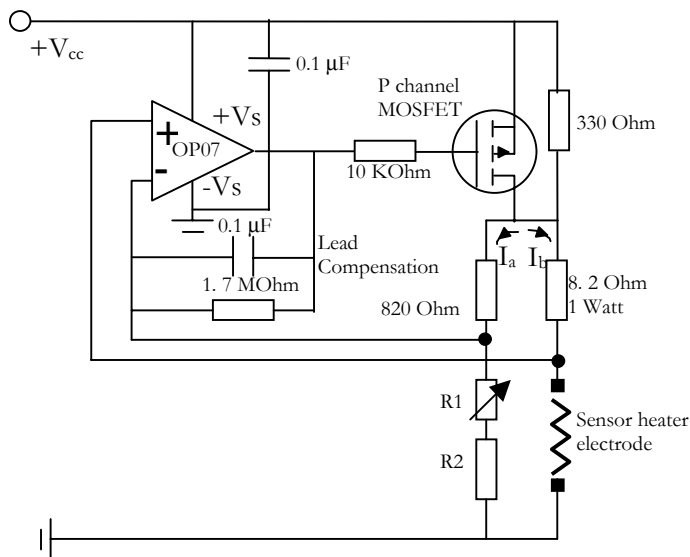


Figure 5.10. Circuit diagram of temperature controller. The resistance of the heater electrode varies linearly with its temperature. A constant reference signal for the regulator is adjusted by varying the value of R1.

This regulator concept is only suited for a constant reference temperature or for temperature gradients with small variations. The reason is that the voltage potential  $V_{cc}$  in figure 5.10. determines a conceivable operation point. As much as possible of the

## 5. Experimental – gate voltage pulsed operation and temperature control

power dissipation should be across the sensor heater electrode. To achieve this the resistance of the current path  $I_a$  must be much larger than  $I_b$ . Further, the resistance serially coupled with the sensor heater electrode must be very low. The imbalance of this Whetstone bridge has the disadvantage that a change in sensor heater resistance causes a relatively small change in voltage difference as input to the operational amplifier and is therefore more sensitive to electronic noise. Since the output load of the operational amplifier is totally capacitive a lead compensate circuit is well suited for stabilisation (U.Tietze, Ch. Schenk, 1993). Further, the proportional part of the lead compensate circuit is large.

P-channel MOSFET characteristics:

---

### MAXIMUM RATINGS (datasheet 6)

$V_{GS}$  : 60 V.

$R_{DS}$  (ON) : 0.55 ohm.

$I_D$  Cont @ 25C : 3 Amps.

$I_D$ (pulsed) : 12 Amps.

$P_D$  20 W.

$T_r/T_f$  (typical) 20/85 ns.

---

$V_{GS}$ , Turn-on voltage :  $\sim -1$  V.  
(experimentally verified)

---

## 5. Experimental – gate voltage pulsed operation and temperature control

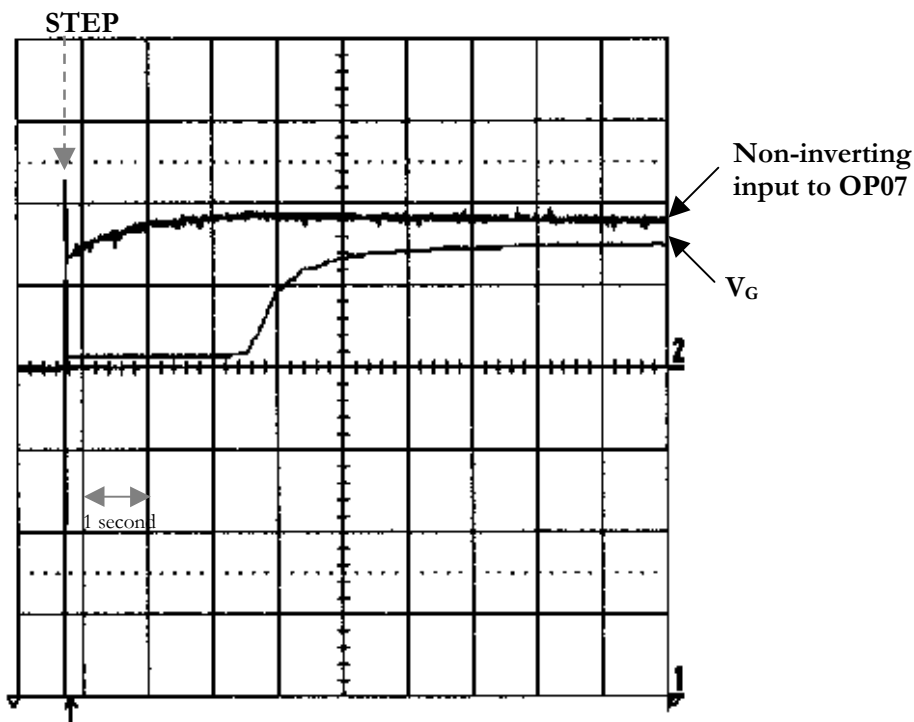


Figure 5.11. Typical response of a temperature step. The uppermost curve corresponds to the non-inverting input of the operational amplifier (200 mV/square). The other curve corresponds to the gate voltage,  $V_G$  (5 V/square). The resistance of the heater electrode slowly increases at the step. Therefore, the voltage to the non-inverting input (one output of the Whetstone bridge) gradually increases. The gate to source voltage,  $V_{GS}$ , reaches a new level when the chip temperature is near the correct operation point, that is  $V_{GS}$  start to decrease, which is seen as an increase in  $V_G$ .

The purpose of the controller is to maintain a specific temperature for variations in the ambient temperature. The voltage potential  $V_{cc}$  for the regulator must be higher than the voltage needed to achieve the correct temperature of the heater electrode. A simple experiment to keep the heater electrode of a MOSFET gas sensor at approximately 100°C has been performed with this regulator. The voltage needed to achieve this temperature was 8.0 V when the ambient atmosphere had room temperature. A step response setting the voltage potential  $V_{cc}$  to 9.5 V is shown in figure 5.12.

## 5. Experimental – gate voltage pulsed operation and temperature control

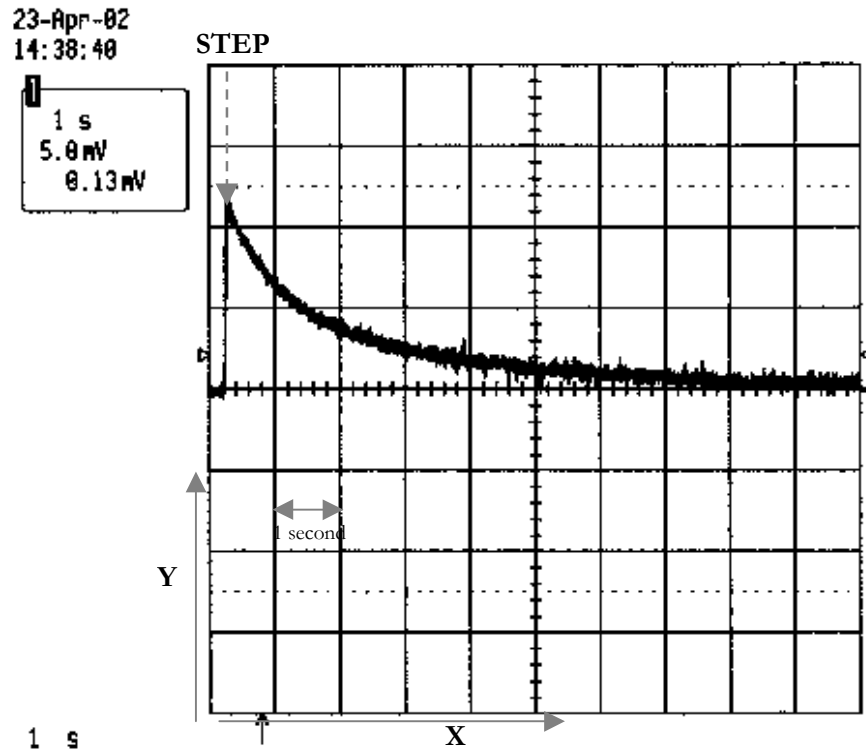


Figure 5.12. Step response from room temperature to  $\sim 100^{\circ}\text{C}$ . The voltage is measured at the output of the Whetstone bridge. One square corresponds to 5.0 mV in Y-direction and 1 second in X-direction.

The electronic mechanism of the regulator can basically be described as follows. When the heater electrode is too warm the FET gate to source potential,  $V_{GS}$ , will increase (influences from filter dynamic disregarded). Thus, the channel of the p-type FET is strangled, leading to less current through the heater electrode. The opposite effect occurs when the heater electrode is too cold. The main factor that influences the step time of a large temperature step is the limit of the control signal, that is the maximum voltage over the heater electrode. A PI-controller using larger control signals has been proven to be faster. However, measurements with temperature disturbances showed that the output from the Whetstone bridge remains zero. The oscillating behaviour in figure 5.12 originate, mainly, from measurement noise.

## 5. Experimental – gate voltage pulsed operation and temperature control

---

A static model for the heater resistance is:

$$R(T) = R_0 \cdot (1 + \alpha(T - T_0)) = R_0 \cdot (1 + \alpha\beta P) = R_0 \cdot (1 + \alpha\beta VI)$$

$R_0$  : Reference resistance.

$T_0$  : Reference temperature.

$\alpha, \beta$  : Constants.

$P$  : Power dissipation of the heater.

$V$  : Voltage across heater electrode.

$I$  : Current through heater electrode.

Three issues that must be emphasised about this regulator are:

- An advantage of this regulator is that it consists of few components. One of the most important considerations to use a controller consisting of as few components as possible is the opportunity to integrate the controller onto the chip. However, this will change the system behaviour slightly. The heat produced by all components will affect the chip temperature, mainly the resistance serially coupled with the heater electrode and the MOSFET, in addition to the heater electrode.
- The controller works well for a "slow" sensor. Almost any regulator aimed to control a constant reference signal to a slow system is robust. Hence, a simple design should be enough. The behaviour for a "fast" sensor, that is a sensor with membrane structure, is not examined.
- The regulator controls the temperature of the heater electrode. For this regulator concept the heater element must be located near the sensor.

## **5. Experimental – gate voltage pulsed operation and temperature control**

### 6. Measurements and conclusions

This chapter presents the results of the performed gas sensing experiments with the produced gas sensor devices. Hydrogen, carbon monoxide and nitrogen dioxide were used as test gases for this purpose.

#### 6.1 Source-drain characteristics of the Insulated-gate TFT

As a first step of characterisation of the produced devices the source-drain characteristics were measured with a HP 4145B Semiconductor Parameter Analyzer. As intended, the drain current was modulated by the gate voltage. The current/voltage characteristics of the IGFET-TFT is shown in figure 6.1, where the drain current is plotted as a function of the source-drain voltage for various gate voltages. A positive gate voltage leads to higher carrier concentration in the channel of the FET, whereas a negative gate voltage leads to electron depletion in the SnO<sub>2</sub> layer.

## 6. Measurements and conclusions

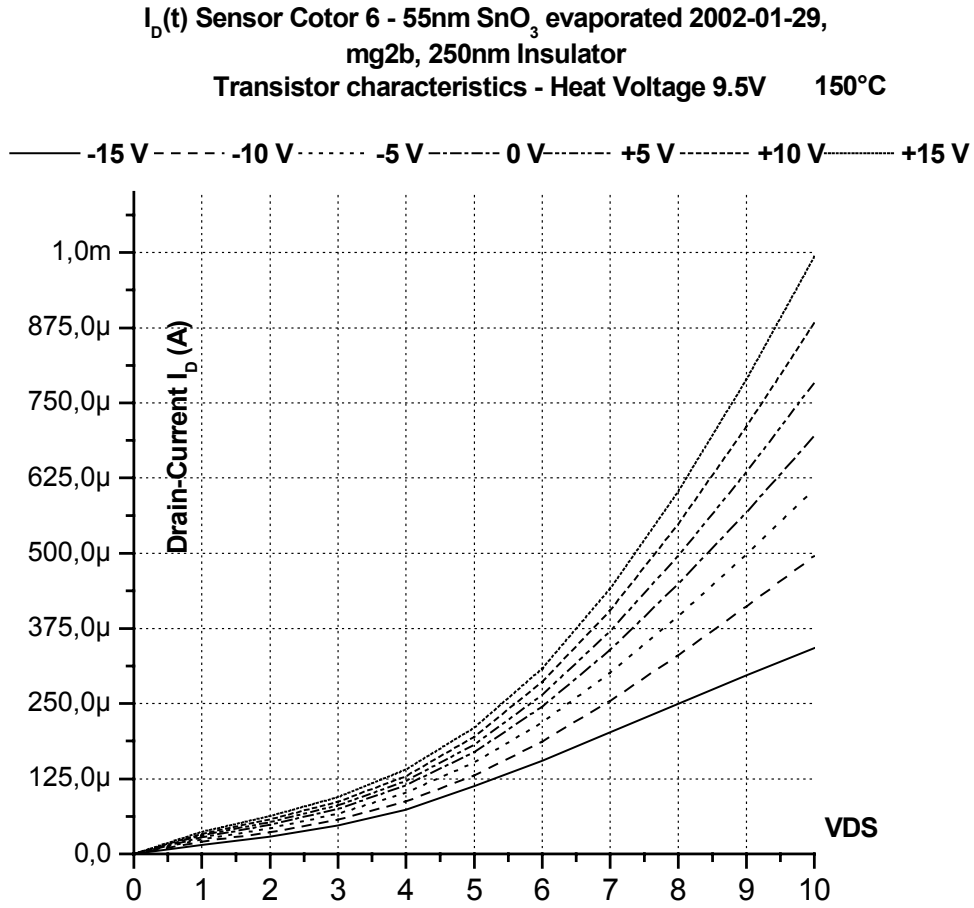


Figure 6.1. Experimental drain characteristics of an SnO<sub>2</sub> (250 nm Si<sub>3</sub>N<sub>4</sub>, layout *mg2b*) based IGFET-TFT ( $T = 150^\circ\text{C}$ ). The gate voltage is varied from -15 V to 15 V in 5 V steps.

### 6.2 Gas measurement proceedings

Gas measurements were performed in the gas measurement laboratory at Fraunhofer IPM. This chapter is mainly focused on gas measurement results of the SnO<sub>2</sub> sensors (250 nm Si<sub>3</sub>N<sub>4</sub>), whose metal oxide is deposited by evaporation, since the sensors with metal oxides deposited by sputtering are not optimal. The tungsten trioxide and the tin dioxide sensors are too high-resistive and too low-resistive, respectively.

It is possible to control the gas concentrations of the gas chamber in the gas laboratory by mass flow controllers. The gas measurements, with gases in magnitude of ppm, were measured in synthetic air of 20% oxygen (O<sub>2</sub>)/80% nitrogen (N<sub>2</sub>) with 50% relative humidity @25°C.

It is reasonable to expect that the sensitivity and the selectivity of gases can be controlled by varying the operation point of the transistor. A positive bias voltage should theoretically increase the adsorption of reducing gases. Since a positive bias voltage potential increases the metal oxide conductivity  $V_{DS}$  have to be quite low to accomplish a good base line. The base line is defined as the sensor signal in pure humidified synthetic air (20% O<sub>2</sub>, 80% N<sub>2</sub>, 50 % r.H.@25°C). A negative bias voltage should theoretically increase the adsorption of oxidising gases. A higher  $V_{DS}$  might be needed in this case to compensate the new operation region. The aim is to have a specified desired gas sensitivity and at the same time high gas selectivity. To be able to weaken the gas sensitivity is also important, because it arises the possibility to measure gases within a wide concentration range. These effects will be discussed for the three different test gases.

A programmable HP Semiconductor Parameter Analyzer, 4145B, is being used to perform the measurements. At each operation point the HP Analyzer applies the transistor electrode potentials and measures the current through the sensor element. A so-called long integration time has been used for the measurements. Gate voltage pulsed operation and this measurement procedure have some similarities. However, the current level is in this case integrated during ~0.5 second at each operation point, normalised to the number of readings, as soon as a specific operation point is set. For the purpose to analyse the mentioned effects above for static operations the measurements presented should only be used as guide-lines for the sensor behaviour, since the sensor needs time to reach equilibrium level.

## 6. Measurements and conclusions

---

### 6.3 Gas measurement

Two sensors, one tungsten trioxide and one tin dioxide sensor are measured at an operation temperature at approximately 200°C. The operation temperature was kept at ~200°C for several days before the measurement was started. Both sensors have ten gates and are denoted *mg2b* (name of the layout). The gate structure of this sensor layout is shown in figure 4.9. The measurement lasts 50 hours and the sensor signal is measured once every second minute for both sensors. The operation points for each single measurement are:

$V_{DS}=1\text{ V}$	$V_{DS}=2\text{ V}$
$V_{GS}=-15$	$V_{GS}=-15\text{ V}$
$V_{GS}=-10$	$V_{GS}=-10\text{ V}$
$V_{GS}=-5$	$V_{GS}=-5\text{ V}$
$V_{GS}=0$	$V_{GS}=0\text{ V}$
$V_{GS}=+5\text{ V}$	$V_{GS}=+5\text{ V}$
$V_{GS}=+10\text{ V}$	$V_{GS}=+10\text{ V}$
$V_{GS}=+15\text{ V}$	$V_{GS}=+15\text{ V}$

First, the operation points in the left column are performed from  $V_{GS}$  at -15 V to gradually increased values up to +15 V. Directly afterwards, the operation points in the right column are performed in the same manner. All ten gates for both sensors are applied to the same voltage potential during the measurement.

#### 6.3.1 Sensor response to hydrogen

The sensors were exposed to three different hydrogen concentrations; 10 ppm, 50 ppm, and 100 ppm  $H_2$ . Each period of gas exposure lasts two hours. Two hours with a "clean" synthetic air mixture are being used before each new gas exposure phase.

The result is shown in figure 6.2 ( $V_{DS}=2\text{ V}$ ,  $SnO_2$  sensor). The uppermost curve corresponds to  $V_{GS}=+15\text{V}$  and the bottom curve to  $V_{GS}=-15\text{V}$ . Hydrogen is a reducing gas and, consequently, the drain current increases during the exposure. The sensor signal returns to its base line when the hydrogen gas flow is switched off.

## 6. Measurements and conclusions

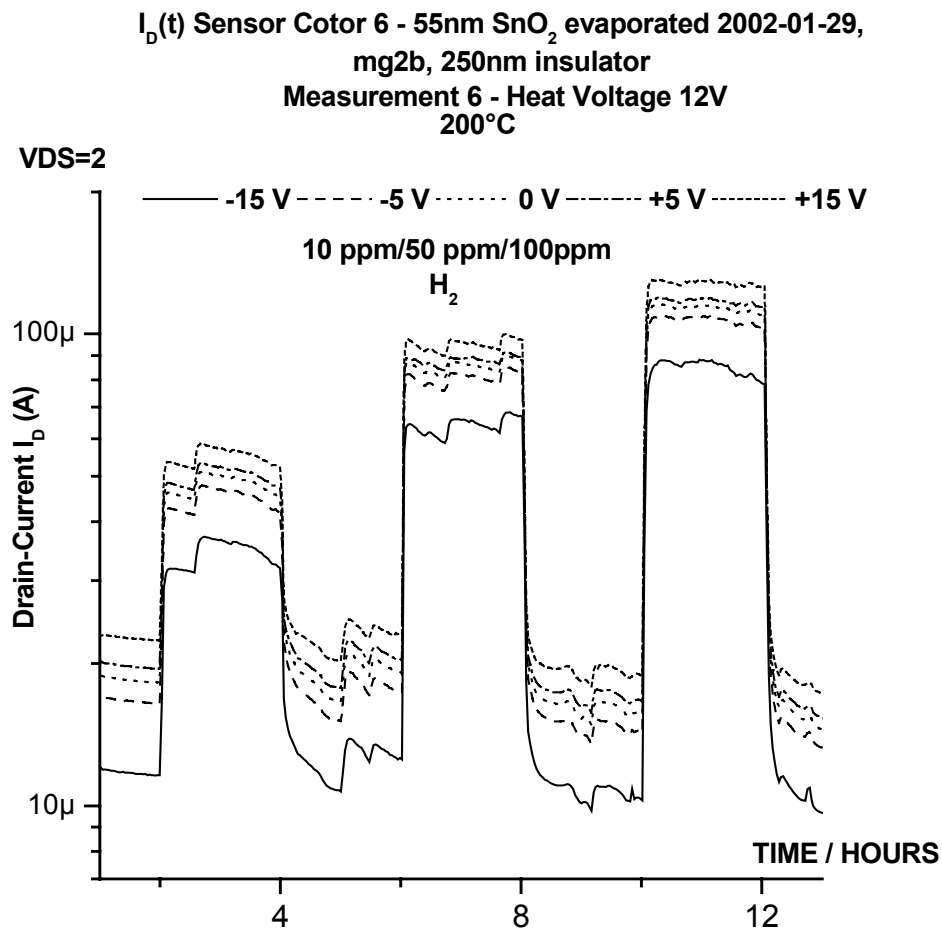


Figure 6.2. Sensor response to different hydrogen concentrations in synthetic air (50% r.H.@25°C). The drain current, in y-direction, is represented logarithmically.  $V_{GS}$  at  $-15$  V,  $-5$  V,  $0$  V,  $+5$  V and  $+15$  V are diagrammed. The device temperature during the experiment was kept at  $200^\circ\text{C}$ .

A more interesting representation of the sensor response is the signal increase in relation to the base line, so-called sensitivity (figure 6.3). Not only does a changed bias voltage potential change the transistor's operation region, but also the quantitative gas reaction at the metal oxide surface. A small sensitivity alteration with varied gate voltage potentials can be observed in figure 6.3.

A gas measurement has also been performed at an operation temperature at approximately  $280^\circ\text{C}$ . The result for this measurement is shown in figure 6.4 and shows the sensor response to all three test gases. The most notable difference between the two temperatures is that the conductivity of the sensor is more controllable for the higher operation temperature. The difference in conductivity is only around a factor 3 between  $V_{GS}=-15$  V and  $V_{GS}=+15$  V at  $\sim 200^\circ\text{C}$ . The same factor is near 100 for the

## 6. Measurements and conclusions

higher operation temperature. Further, the sensitivity to hydrogen varies much more at  $\sim 280^\circ\text{C}$  (high for  $V_{GS} = -15\text{ V}$  and lower for  $V_{GS} = +15\text{ V}$ ).

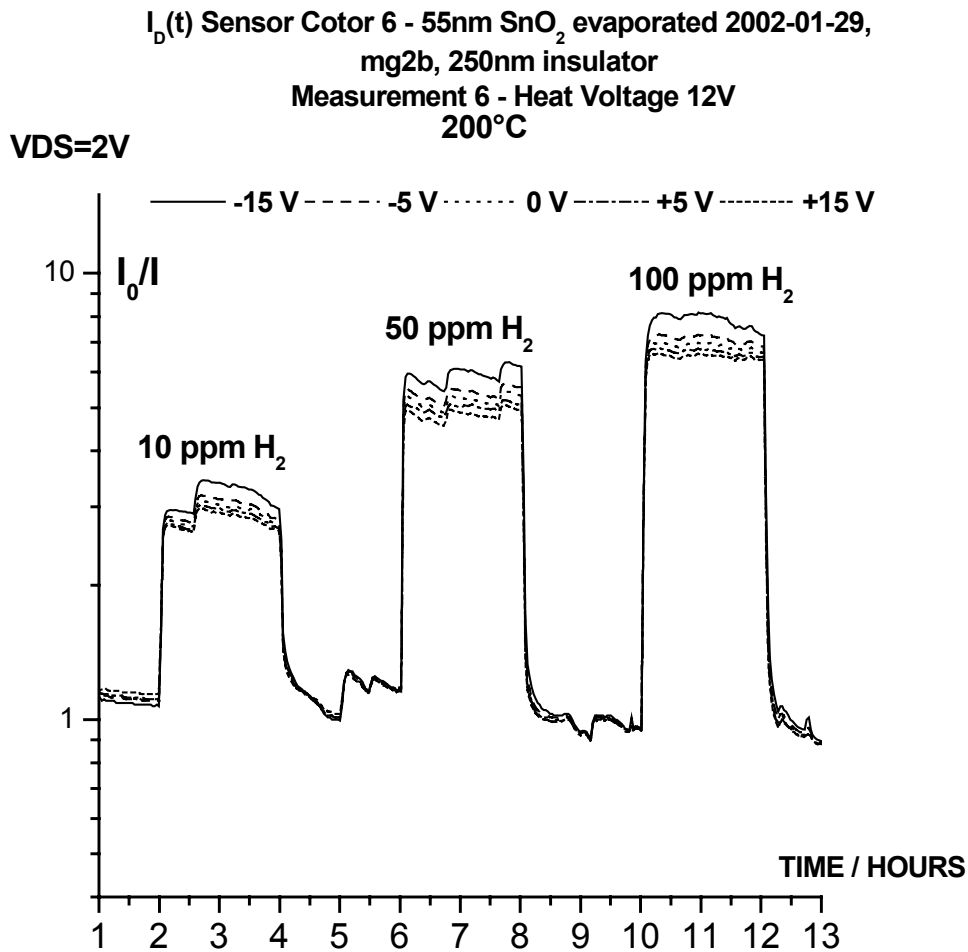


Figure 6.3. Sensitivity variations to hydrogen for different gate voltage potentials. The gas sensitivity is here defined as  $I/I_0$  ( $I$  : drain current for gas exposure,  $I_0$  : drain current at base line). The sensitivity, in y-direction, is represented logarithmically.  $V_{GS}$  at  $-15\text{ V}$ ,  $-5\text{ V}$ ,  $0\text{ V}$ ,  $+5\text{ V}$  and  $+15\text{ V}$  are diagrammed. The device temperature during the experiment was kept at  $200^\circ\text{C}$ .

## 6. Measurements and conclusions

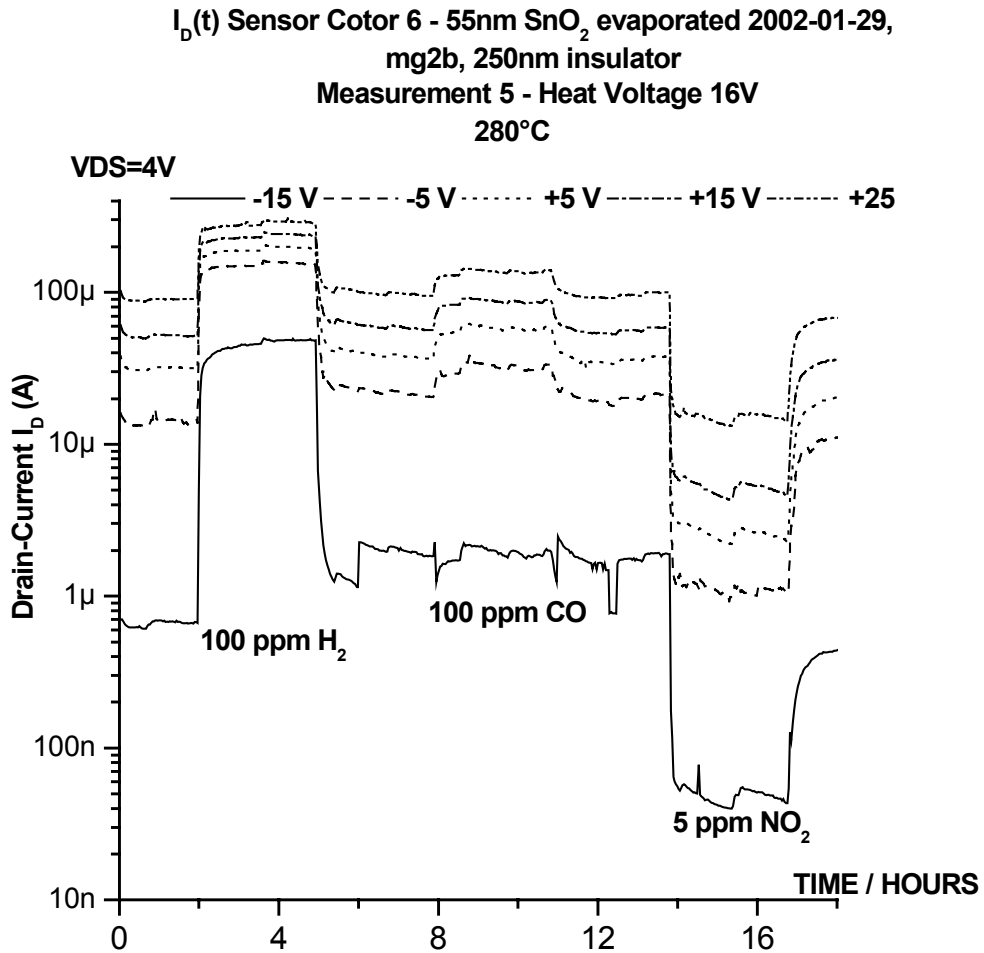


Figure 6.4. Sensor response to hydrogen, carbon monoxide and nitrogen dioxide. Since nitrogen dioxide is an oxidising gas it causes a decrease in drain current.  $V_{DS}$  is set to 4 V.  $V_{GS}$  varies between -15 V and +25 V (all gate potentials identical). The device temperature during the experiment was kept at 280°C.

## 6. Measurements and conclusions

### 6.3.2 Sensor response to carbon monoxide

The measurement proceeds with carbon monoxide as test gas. The same gas concentrations as for hydrogen are being used; 10 ppm, 50 ppm and 100 ppm.

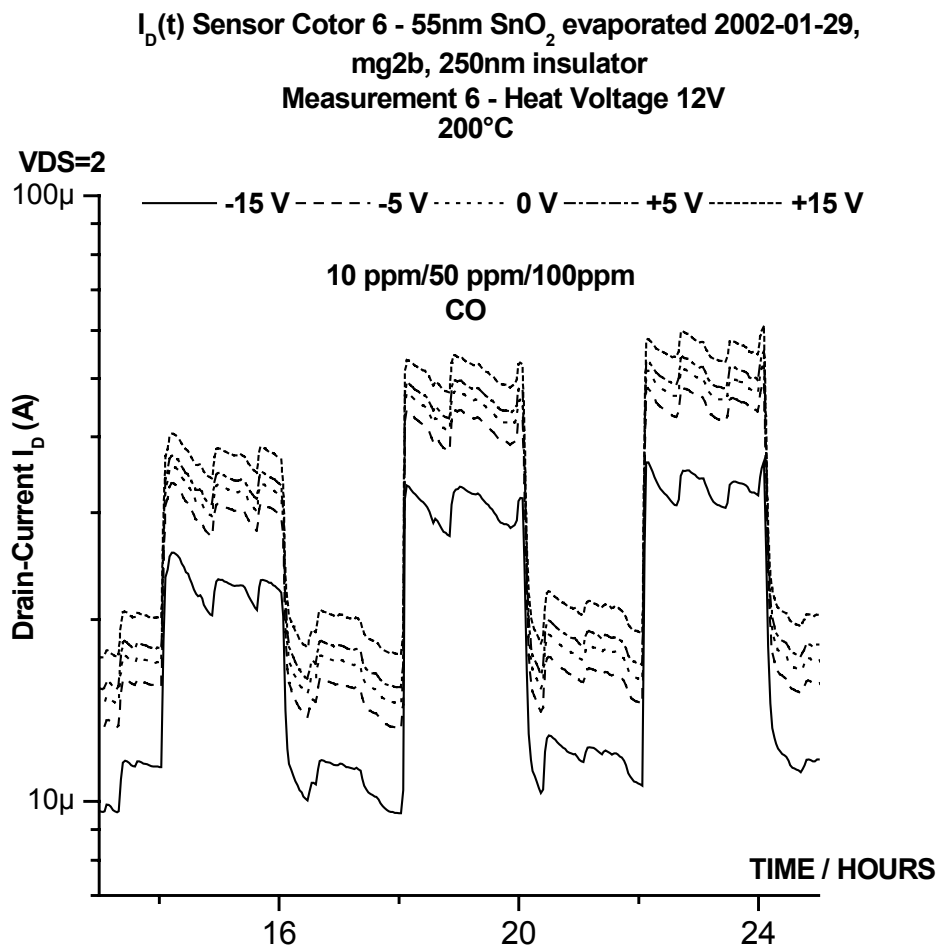


Figure 6.5. Sensor response to different carbon monoxide concentrations in synthetic air (50% r.H.@25°C). The drain current, in y-direction, is represented logarithmically.  $V_{GS}$  at -15 V, -5 V, 0 V, +5 V and +15 V are diagrammed. The device temperature during the experiment was kept at 200°C.

The sensitivity diagram for carbon monoxide, at ~200°C, shows small alterations for different applied gate voltage potentials. The sensitivity to carbon monoxide remains at the same magnitude also at ~280°C when the bias voltage potential is varied from -5 V to +25 V ( $V_{DS} = 4$  V).

## 6. Measurements and conclusions

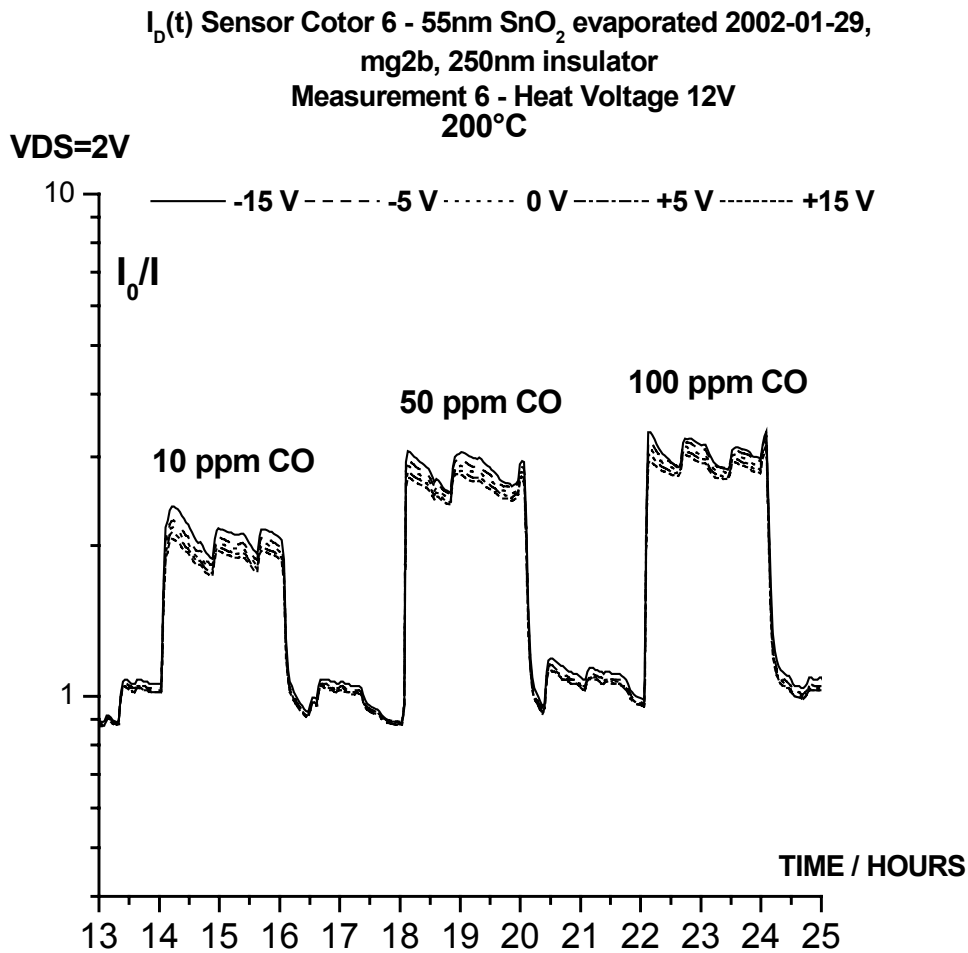


Figure 6.6. Sensitivity variations to carbon monoxide for different gate voltage potentials. The gas sensitivity is here defined as  $I/I_0$  ( $I$ : drain current for gas exposure,  $I_0$ : drain current at base line). The sensitivity, in y-direction, is represented logarithmically. The device temperature during the experiment was kept at 200°C.

The sensitivity remains at the same magnitude for different applied gate voltage potentials (-15 V to +15 V), although the transistor's operation region changes, for both H<sub>2</sub> and CO ( $V_{DS} = 2$  V,  $\sim 200^\circ\text{C}$ ).

## 6. Measurements and conclusions

### 6.3.3 Sensor response to nitrogen dioxide

Nitrogen dioxide is, in contrast to hydrogen and carbon monoxide, an oxidising gas. This gas will take conducting electrons from the metal oxide. Hence, the drain current decreases by exposure. Two concentrations are being tested in the measurement; 2 ppm and 5 ppm.

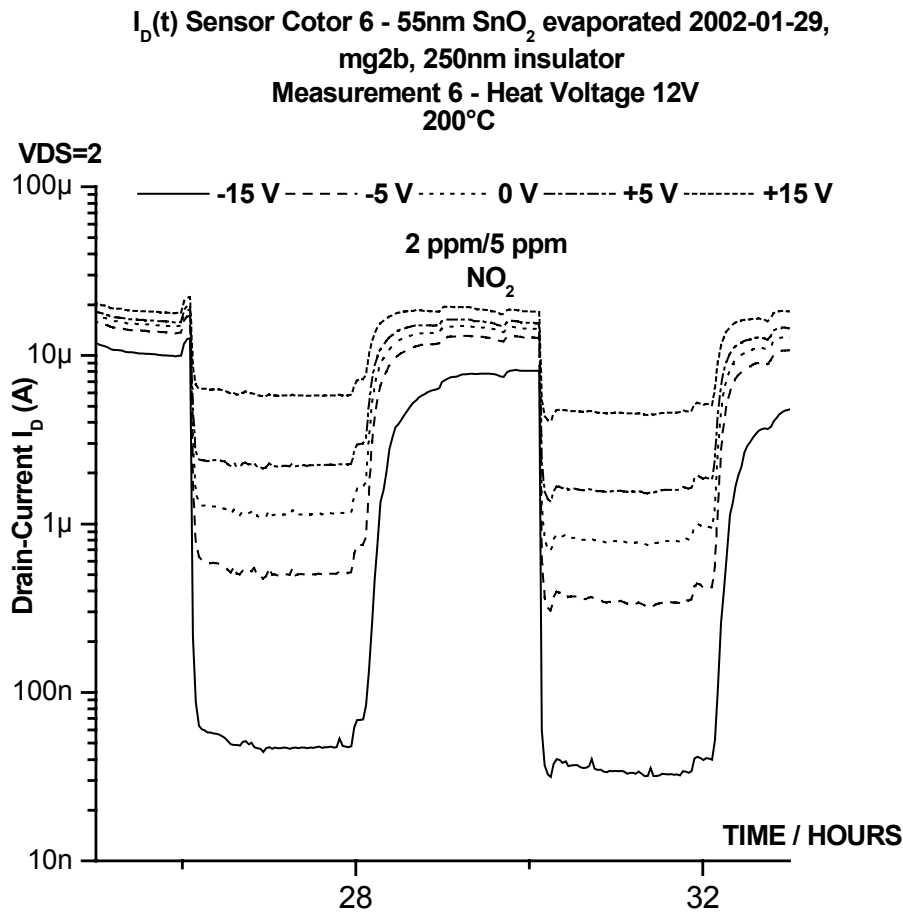


Figure 6.7. Sensor response to two different nitrogen dioxide concentrations in synthetic air (50% r.H.@25°C). The drain current, in y-direction, is represented logarithmically.  $V_{GS}$  at -15 V, -5 V, 0 V, +5 V and +15 V are diagrammed. The device temperature during the experiment was kept at 200°C.

Already by looking at figure 6.7 it is clear that the sensitivity increases enormously for negative gate voltage potentials. The sensitivity diagram is shown in figure 6.8. The gas sensitivity in this figure is the inverse relationship to the previous defined sensitivity quote.

## 6. Measurements and conclusions

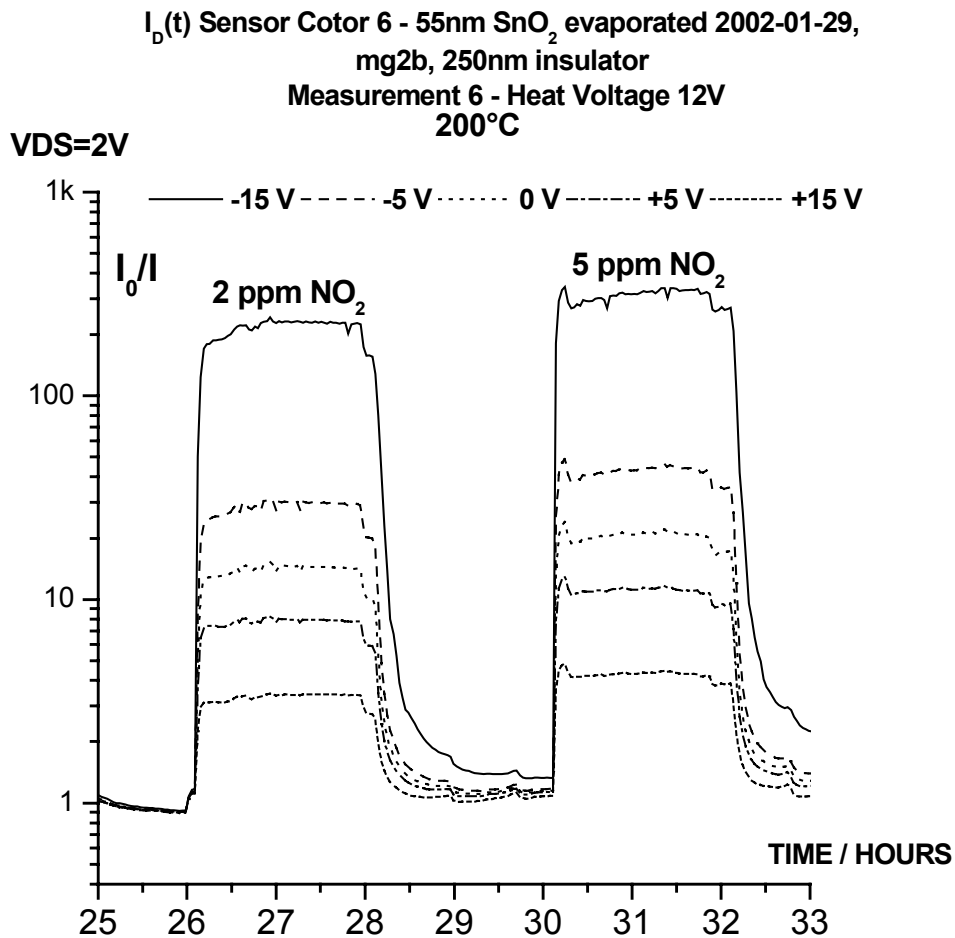


Figure 6.8. Sensitivity variations to nitrogen dioxide for different gate voltage potentials. The gas sensitivity is here defined as  $I_0/I$  ( $I$  : drain current for gas exposure,  $I_0$  : drain current at base line). This is the inverse relationship to the definition made in figure 6.3 and 6.6. The sensitivity, in y-direction, is represented logarithmically. The device temperature during the experiment was kept at 200°C.

### 6.3 Summary and Conclusions

The aim of the thesis was to investigate the influence of an applied external electric field on the gas sensing properties of thin-film metal oxides. The first step was the development of new technologies for an Insulated-gate thin-film transistor based on thin-film metal oxides as semiconducting material. The following electrical characterisation revealed that the conductivity of the produced transistor devices, for both tin dioxide sensors (deposited by evaporation) and tungsten trioxide sensors (deposited by sputtering), can be modulated by an applied bias voltage potential.

The performed gas measurements indicated that the sensors can detect reducing (e.g. hydrogen and carbon monoxide) and oxidising (e.g. nitrogen dioxide) gases. The conductivity of the sensor with sputtered tungsten trioxide (*mg2b*, 125 nm  $\text{WO}_3$ , 150 nm  $\text{Si}_3\text{N}_4$ ) is well controllable at  $\sim 200^\circ\text{C}$  and  $\sim 280^\circ\text{C}$ . However, for a negative gate voltage potential the tungsten trioxide sensor hardly detects any gases, because it is too high-resistive. The sensor with sputtered tin dioxide (*mg1b*, 75 nm  $\text{SnO}_2$ , 150 nm  $\text{Si}_3\text{N}_4$ ), on the other hand, is far too low-resistive. The sensor with evaporated tin dioxide (*mg2b*, 55 nm  $\text{SnO}_2$ , 250 nm  $\text{Si}_3\text{N}_4$ ) shows much more desirable gas sensing properties. The sensitivity to hydrogen, defined as  $I/I_0$ , and nitrogen dioxide, defined as  $I_0/I$ , is higher for negative gate voltage potentials at  $\sim 280^\circ\text{C}$  and at  $V_{\text{DS}} = 4\text{ V}$  for this sensor. Further, the sensitivity to carbon monoxide, defined as  $I/I_0$ , remains at the same magnitude for gate voltage potentials from  $-5\text{ V}$  to  $+25\text{ V}$  at  $\sim 280^\circ\text{C}$  and at  $V_{\text{DS}} = 4\text{ V}$ .

One important task was to investigate the sensor performance at lower temperatures. This is important when considering to integrate electronics for processing of the measurements onto the chip, therefore a measurement at  $\sim 200^\circ\text{C}$  has been performed. This measurement shows that although the conductivity changes for different bias voltage potentials, the sensitivity remains at the same magnitude for hydrogen and carbon monoxide at  $V_{\text{DS}} = 2\text{ V}$ . An interesting property of this sensor is that the sensitivity to nitrogen dioxide is very well controllable at  $\sim 200^\circ\text{C}$ . The sensitivity to nitrogen dioxide is strongly influenced by an applied bias voltage potential. Negative gate voltage potentials lead to a significant increase of the nitrogen dioxide sensitivity. For example, the sensitivity to 2 ppm  $\text{NO}_2$  increases from a value of  $\sim 13$  for an applied gate voltage potential of 0 V to  $\sim 200$  for an applied gate voltage potential of  $-15\text{ V}$ .

## 7. Outlook

Some suggestions for future work are:

### **Measurements :**

Find the optimal operation points ( $V_{DS}$ ,  $V_{GS}$ ) where the sensitivity is optimal and the selectivity is high. It is likely that the Fermi level of the metal oxide bulk can be modulated by applying different gate voltage potentials to the different gate electrodes. To study how the sensor behaviour is affected for this condition is also interesting.

Investigate the influence of external electric fields on the gas response time. It is likely that an applied gate potential will speed up the desorption of gas molecules from the sensor surface and hence the recovery of the sensor signal after gas exposure. Gate voltage pulsed operation can be used to study this.

Finally, how does the operation temperature affect the sensor properties?

### **Materials :**

Try with a thicker tungsten trioxide layer (more than 125 nm) and make new attempts to deposit tin dioxide with a sputtering procedure.

The thickness of the insulator, silicon nitride, is also an important material parameter. A thinner layer might result in less bias voltage potential needed to achieve optimal sensitivity and high selectivity. This is an important issue for a possible commercial sensor.

### **Simulation and calculations :**

Simulate how the surface coverage of adatoms (e.g. oxygen) are influenced on electric fields.

Perform FEM-simulations of the field distribution across gate and semiconducting channel.

Modelling of the developed sensor as transistor and as gas sensor.

**7. Outlook**

---

### Settings for gate voltage/temperature pulsed operation

1. Choose operation mode by setting the switch (*TPO/GVPO*) at the front panel. **Temperature pulsed operation (*TPO*)**, **gate voltage pulsed operation (*GVPO*)**.
2. If gate voltage pulsed operation mode is used one must select positive or negative pulsed mode by setting the switch (*GVPO+/GVPO-*) at the front panel. The position of the jumper at the PCB labelled (*GVPO+/GVPO-*) must also be set at the chosen pulsed mode.
3. The position of the jumper at the PCB labelled (*>50%* , *<50%*) determines if the duty cycle used should be more or less than 50 %. The setting is valid for both gate voltage pulsed operation and temperature pulsed operation.
4. Adjust the length of the trigger pulse by turning the potentiometer at the PCB labelled *Trigger*. The setting is valid for both gate voltage pulsed operation and temperature pulsed operation.
5. Adjust the duty cycle and the period time of the pulse by turning the potentiometers at the PCB labelled  $R_A$  and  $R_B$ . It is easiest to first adjust the two potentiometers labelled  $R_B$  to achieve a near to correct time for pulse time  $T_{high}$ , which is the time for high level if more than 50 % duty cycle is set ( $T_{low}$  if less than 50 % duty cycle is set). At the next step, adjust the potentiometers labelled  $R_A$  to achieve correct period time. Finally, to achieve the exact values all potentiometers, both  $R_A$  and  $R_B$ , have to be adjusted. The setting is valid for both gate voltage pulsed operation and temperature pulsed operation.
6. For the trigger pulse external voltage sources, the inputs  $Tr+$  and  $Tr-$  at the front panel, are needed. The output is TTL compatible for a voltage potential at 5 V ( $Tr+ = 5$  V,  $Tr- = 0$  V). The output for the trigger pulse is labelled *Trigg* at the front panel.
7. The outputs for gate voltage potentials and heat voltage potential for temperature pulsed operation are connected to the output pins at the PCB. The ground level for all these voltage potentials are labelled *GROUND* at the front panel.



### DEPOSITION OF TANTALUM/PLATINUM

#### Evaporation of Al as sacrificial layer

Target : 3 quarters of 6 inch wafers COTOR – 150 nm Si<sub>3</sub>N<sub>4</sub>, 200 nm Si<sub>3</sub>N<sub>4</sub>, 250 nm Si<sub>3</sub>N<sub>4</sub>.

Date : 2001-12-12 / 2002-01-14.

Estimated final thickness : 2800 Å .

#### Photolithographic process for sensor electrodes and heater electrode/temperature sensor

Target : 3 quarters of 6 inch wafers COTOR – 150 nm Si<sub>3</sub>N<sub>4</sub>, 200 nm Si<sub>3</sub>N<sub>4</sub>, 250 nm Si<sub>3</sub>N<sub>4</sub> .

Date : 2001-12-13, 2001-12-17 / 2002-01-14.

Photoresist: AZ 5214.

Spin speed for photoresist deposition : 3000 rpm.

Heating after photoresist deposition: 90°C, 20 min.

Contact mode : SOFT CONTACT.

Light power : 40 mJ/cm<sup>2</sup>.

Exposure time : 5.8 s.

Developer liquid : AZ Developer, 50% Developer – 50 % H<sub>2</sub>O, 23°C.

Development time : 90 s.

Air humidity : 45 %.

#### Wet etching of TaPt structures

Target : 3 quarters of 6 inch wafers COTOR – 150 nm Si<sub>3</sub>N<sub>4</sub>, 200 nm Si<sub>3</sub>N<sub>4</sub>, 250 nm Si<sub>3</sub>N<sub>4</sub> .

Date : 2001-12-18 / 2002-01-18.

Heating before the wet etching: 120°C, 60 min.

600 ml liquid :

H <sub>2</sub> O	10 % (60 ml)
H <sub>3</sub> PO <sub>4</sub> (85%)	80 % (480 ml)
CH <sub>3</sub> COOH(100%)	5 % (30 ml)
HNO <sub>3</sub> (69%)	5 % (30 ml)

Wet etching : 40°C, 4 min.

Time needed to etch through the aluminium layer : 75 s.

## **Appendix B – Protocol for backend process**

---

### **Evaporation of TaPt**

Target : 3 quarters of 6 inch wafers COTOR – 150 nm Si<sub>3</sub>N<sub>4</sub>, 200 nm Si<sub>3</sub>N<sub>4</sub>, 250 nm Si<sub>3</sub>N<sub>4</sub> .

Date : 2001-12-21 / 2002-01-18.

Estimated final tantalum thickness : 250 Å .

Estimated final platinum thickness : 2000 Å .

Evaporated according to Fraunhofer IPM standard process for TaPt.

### **Lift-off process for TaPt**

Target : 3 quarters of 6 inch wafers COTOR – 150 nm Si<sub>3</sub>N<sub>4</sub>, 200 nm Si<sub>3</sub>N<sub>4</sub>, 250 nm Si<sub>3</sub>N<sub>4</sub> .

Date : 2001-12-21 / 2002-01-24.

Liquid for lift-off process :

1. Acetone Puranal – a small amount of ultrasonic.
2. Isopropanol Puranal.

### **Removal of the sacrificial aluminium layer**

Target : 3 quarters of 6 inch wafers COTOR – 150 nm Si<sub>3</sub>N<sub>4</sub>, 200 nm Si<sub>3</sub>N<sub>4</sub>, 250 nm Si<sub>3</sub>N<sub>4</sub> .

Date : 2002-01-07 / 2002-01-25

Same process parameters as for wet etching of TaPt structures, except the etching time.

Wet etching : 40°C, 10 min.

### DEPOSITION OF METAL OXIDE

#### Photolithographic process for metal oxide

Target : 3 quarters of 6 inch wafers COTOR – 150 nm Si<sub>3</sub>N<sub>4</sub>, 200 nm Si<sub>3</sub>N<sub>4</sub>, 250 nm Si<sub>3</sub>N<sub>4</sub>.

Date : 2002-01-09 / 2002-01-25.

Same process parameters as for photolithographic process for sensor electrodes and heater electrode/temperature sensor, except 30 min HMDS (Hexamethyl disilazane) before photoresist deposition.

#### Sputtering of tin dioxide

Target : 2 quarters of 6 inch wafers COTOR – 150 nm Si<sub>3</sub>N<sub>4</sub>, 200 nm Si<sub>3</sub>N<sub>4</sub>, 250 nm Si<sub>3</sub>N<sub>4</sub>.

Date : 2002-02-06.

Measured final thickness : 75 nm.

Table : Process parameters for sputtering of tin dioxide.

Parameter	Value
Etch process:	
Argon (mass flow)	1.0 sccm
Background pressure	4*10 <sup>-6</sup> mbar
Process pressure	4.7*10 <sup>-3</sup> mbar
Process time	2*3 min (10 min pause)
Forward power	1.5 kW
Reflected Power	< 200 W
Bias voltage	680-700 V
Pre-sputtering:	
Argon (mass flow)	2.3 sccm
Oxygen (mass flow)	0.6 sccm
Forward power	0.5 kW
Reflected power	~0 W
Process time	5 min
Cathode voltage	125 V
Sputtering:	
Argon (mass flow)	2.3 sccm
Oxygen (mass flow)	0.6 sccm
Background pressure	6*10 <sup>-6</sup> mbar
Process pressure	8.4*10 <sup>-3</sup> mbar
Forward power	0.5 kW
Reflected power	~0 W
Process time	2*6.6 min (10 min pause)
Cathode voltage	113 V

## Appendix B – Protocol for backend process

---

### Evaporation of tin dioxide

Target : 1 piece of 6 inch wafers COTOR - 250 nm Si<sub>3</sub>N<sub>4</sub>.

Date : 2002-01-29.

Measured final thickness : 55 nm.

Evaporated according to Fraunhofer IPM standard process for SnO<sub>2</sub>.

### Sputtering of tungsten trioxide

Target : 3 quarters of 6 inch wafers COTOR – 150 nm Si<sub>3</sub>N<sub>4</sub>, 200 nm Si<sub>3</sub>N<sub>4</sub>.

Date : 2002-01-15.

Measured final thickness : 125 nm.

Table : Process parameters for sputtering of tungsten trioxide.

Parameter	Value
W-target, free sputtering:	
Argon (mass flow)	4.3 sccm
Background pressure	7*10 <sup>-6</sup> mbar
Process pressure	1.2*10 <sup>-2</sup> mbar
Process time	15 min
Forward power	0.5 kW
Reflected Power	~0 W
Cathode voltage	125 V
WO <sub>3</sub> – reactive pre-sputtering:	
Argon (mass flow)	4.9 sccm
Oxygen (mass flow)	2.1 sccm
Forward power	0.25 kW
Reflected power	~0 W
Process time	10 min
Cathode voltage	113 V
WO <sub>3</sub> – reactive sputtering:	
Argon (mass flow)	4.9 sccm
Oxygen (mass flow)	2.1 sccm
Background pressure	6*10 <sup>-6</sup> mbar
Process pressure	1.5*10 <sup>-2</sup> mbar
Forward power	0.25 kW
Reflected power	~0 W
Process time	94 min
Cathode voltage	103 V

# Appendix B – Protocol for backend process

---

## Lift-off process for metal oxide

Target : 3 quarters of 6 inch wafers COTOR – 150 nm Si<sub>3</sub>N<sub>4</sub>, 200 nm Si<sub>3</sub>N<sub>4</sub>, 250 nm Si<sub>3</sub>N<sub>4</sub>.  
Date : 2002-01-16, 2002-01-17 (tungsten trioxide); 2002-01-29 (evaporated tin dioxide);  
2002-02-06 (sputtered tin dioxide)

Liquid for lift-off process :

1. Acetone Puranal – a small amount of ultrasonic.
2. Isopropanol Puranal.

## BOND PARAMETERS

Bond parameters used for the gate pads and platinum pads are:

	Force	Time	Power
Chip	9.0	9.0	7.5
TO5 housing	9.0	9.0	6.0

(gold thread, bond machine from *KULICKE AND SOFFA industries, Inc*)

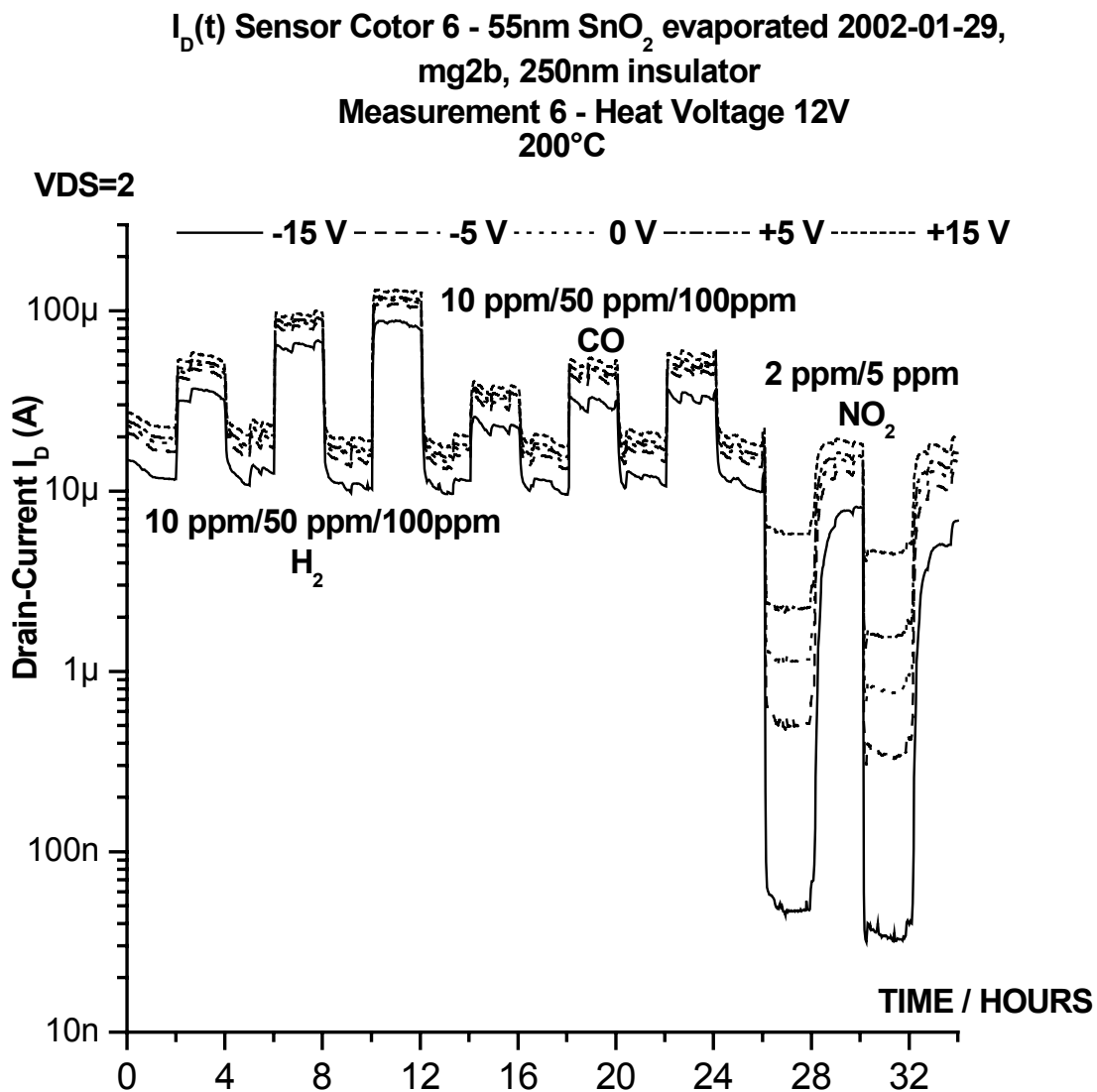
Bond temperature is 170°C.



## Appendix C – Gas measurement

Gas measurement presented in chapter 6. *Measurements and conclusions*

- Operation temperature:  $\sim 200^{\circ}\text{C}$ .
- Layout: *mg2b*.
- Insulator thickness: 250 nm  $\text{Si}_3\text{N}_4$ .
- Metal oxide:  $\text{SnO}_2$  55 nm, evaporated.
- All gate potentials identical.





## REFERENCES

Internet: hyperphysics

URL - <http://hyperphysics.phy-astr.gsu.edu>

Larsson-Edefors P. (2000), *Lecture notes in TFFY34 Semiconductor Technology*, Sweden

URL - [http://www.ifm.liu.se/courses/tffy34/Lectures\\_2000.pdf](http://www.ifm.liu.se/courses/tffy34/Lectures_2000.pdf)

D.A. Grant, J. Gowar (1989), *POWER MOSFETS – Theory and Applications*, USA  
John Wiley & Sons, Inc.

H. Borkan, P.K. Weimer, *An analysis of the characteristics of insulated-gate thin-film transistors*,  
RCA Laboratories, Princeton, N.J.

Internationella Miljöinstitutet Lund, Sweden,

URL - <http://www1 ldc.lu.se/iiiee/EMISSIONS/NOX/NOX.HTML>

U.S. Environmental Protection Agency,

URL - <http://www.epa.gov/otaq/03-co.htm>

W. Hellmich, G. Müller, Ch. Bosch-v, Braunmühl, T.Doll, I.Eisele (1997),

Paper publicised in *Sensor and actuators B : Field-effect-induced gas sensitivity changes in metal oxides*.

J. Wöllenstein, M. Jäggle, H. Böttner, *A gas sensitive tin dioxide thin-film transistor*, Germany

Paper publicised at Fraunhofer Institute of Physical Measurement Techniques.

H.Geistlinger (1993),

Paper publicised in *Sensor and actuators B : Electron theory of thin-film gas sensors*.

Elmasry M.I (1994), *BiCMOS Integrated Circuit Design*, USA

IEEE PRESS.

J.Wöllenstein (1997), Diplomarbeit

*"Herstellung und Charakterisierung von SnO<sub>2</sub>-Feldeffektkonfigurationen"*

Publicised by Universität Gesamthochschule Kassel, Institut für periphere Mikroelektronik  
Elektrische Messtechnik.

A.Pohlmann (2001), Diplomarbeit

*"Herstellung und Charakterisierung von Metalloxid-Sensorsarrays auf Silicium-Substrat"*

Publicised by Fachhochschule Furtwangen, University of Applied Physics.

R. E. Cavicchi, J.S. Suehle, K. G. Kreider, M. Gaitan, P. Chaparala, (1996),

Paper publicised in *Sensor and actuators B : Optimized temperature-pulse sequences for the enhancement of chemically specific response patterns from micro-hotplate gas sensors*, Chemical 33 (1-3) pp. 142-146.

Datasheet 1:

URL - <http://www.farnell.com/datasheets/6604.pdf>

Datasheet 2:

URL - <http://www.farnell.com/datasheets/5.pdf>

Datasheet 3:

URL - <http://www.farnell.com/datasheets/4838.pdf>

Datasheet 4:

URL - <http://www.farnell.com/datasheets/4815.pdf>

Datasheet 5:

URL - <http://www.farnell.com/datasheets/412.pdf>

Datasheet 6:

URL - <http://www.farnell.com/datasheets/22505.pdf>

Internet: capteur

URL - <http://www.captour.co.uk/>

U.Tietze, Ch. Schenk (1993), "*Halbleiter-Schaltungstechnik*", Springer-Verlag.